Quantum information processing using quasiclassical electromagnetic interactions between qubits and electrical resonators

Quantum information processing using quasiclassical electromagnetic interactions between qubits and electrical resonators

2013 New J. Phys. 15 123011

(http://iopscience.iop.org/1367-2630/15/12/123011)

New Journal of Physics
The open access journal for physics

Quantum information processing using quasiclassical electromagnetic interactions between qubits and electrical resonators

Andrew J Kerman
MIT Lincoln Laboratory, Lexington, MA, USA
E-mail: ajkerman@ll.mit.edu

New Journal of Physics **15** (2013) 123011 (29pp)
Received 12 August 2013
Published 6 December 2013
Online at http://www.njp.org/
doi:10.1088/1367-2630/15/12/123011

Abstract. Electrical resonators are widely used in quantum information processing, by engineering an electromagnetic interaction with qubits based on real or virtual exchange of microwave photons. This interaction relies on strong coupling between the qubits' transition dipole moments and the vacuum fluctuations of the resonator in the same manner as cavity quantum electrodynamics (QED), and has consequently come to be called 'circuit QED' (cQED). Great strides in the control of quantum information have already been made experimentally using this idea. However, the central role played by photon exchange induced by quantum fluctuations in cQED does result in some characteristic limitations. In this paper, we discuss an alternative method for coupling qubits electromagnetically via a resonator, in which no photons are exchanged, and where the resonator need not have strong quantum fluctuations. Instead, the interaction can be viewed in terms of classical, effective 'forces' exerted by the qubits on the resonator, and the resulting resonator dynamics used to produce qubit entanglement are purely classical in nature. We show how this type of interaction is similar to that encountered in the manipulation of atomic ion qubits, and we exploit this analogy to construct two-qubit entangling operations that are largely insensitive to thermal or other noise in the resonator, and to its quality factor. These operations are also extensible to larger numbers of qubits, allowing interactions to be selectively generated among any desired

subset of those coupled to a single resonator. Our proposal is potentially applicable to a variety of physical qubit modalities, including superconducting and semiconducting solid-state qubits, trapped molecular ions, and possibly even electron spins in solids.

Contents

1. Introduction

Microwave electrical resonators are already an important tool for manipulating quantum information using electromagnetic interactions [1]. As a means of quantum information storage or communication, they are used or proposed in a variety of schemes [2] involving, for example, trapped molecular ions [3], neutral polar molecules [4], Rydberg atoms [5–9], superconducting Josephson-junction qubits [10–13], and electron spins in solids [14, 15]. In nearly all of these cases, the resonator is used in a way familiar from optical cavity quantum electrodynamics [9, 16], in which the qubits exchange real or virtual photons with it, and where the figure of merit is the speed with which this exchange occurs (or equivalently, the strength of the coherent coupling between the qubit's transition dipole moment and the resonator's vacuum fluctuations). In fact, many of the seminal cavity quantum electrodynamics (QED) results have been replicated in a circuit environment, a field now known as circuit QED [10–13] (cQED).

Just as with its optical predecessor, cQED for a single qubit interacting with a resonator can be approximately described by the Jaynes–Cummings model[1], with the Hamiltonian [10, 11]

$$\hat{H}_{\mathrm{JC}} = \frac{\hbar\omega_{\mathrm{q}}}{2}\hat{\sigma}_{\mathrm{q}}^{z} + \hbar\omega_{\mathrm{r}}\left(\hat{a}^{\dagger}\hat{a} + \frac{1}{2}\right) + \hat{H}_{\perp}, \tag{1}$$

where $\hbar\omega_{\mathrm{q}}$ is the energy splitting between the qubit's two states $|e\rangle$ and $|g\rangle$, whose Hilbert space is acted on by $\hat{\sigma}_{\mathrm{q}}^{z}$, and $\hat{a}$ is the annihilation operator for photons of a resonator mode with frequency ω_{r} described by the photon number states $|n\rangle$ such that $\hat{a}|0\rangle = 0$. The transverse interaction is given in the rotating-wave approximation by

$$\hat{H}_{\perp} \approx \hbar g_{\perp}\left(\hat{a}\hat{\sigma}_{\mathrm{q}}^{+} + \hat{a}^{\dagger}\hat{\sigma}_{\mathrm{q}}^{-}\right) \tag{2}$$

[1] See, for example, [17].

where $\hat{\sigma}_q^{\pm} \equiv (\hat{\sigma}_q^x \pm i\hat{\sigma}_q^y)/2$ are the qubit raising and lowering operators, and equation (2) holds approximately as long as the coupling is not too strong: $g_\perp \ll \omega_r, \omega_q$. The coupling strength has the generic form: $\hbar g_\perp = \mu_q \delta F_{rms}$, where $\mu_q \equiv \langle g|\hat{\mu}_q|e\rangle$ is the qubit's transition dipole moment ($\hat{\mu}_q$ is the appropriate electric or magnetic dipole moment operator for the qubit), and δF_{rms} is the rms amplitude of the resonator's electric or magnetic field vacuum fluctuations. Equation (2) then describes an exchange of photons between the qubit and the resonator mode, via interaction between the resonator field and the qubit's dipole moment.

If the detuning between resonator and qubit $\Delta_q \equiv \omega_r - \omega_q$ is much smaller than $g_\perp$, Rabi flopping at frequency $g_\perp$ (described in the frequency domain by the vacuum Rabi splitting) can occur between the states $|e, 0\rangle$ and $|g, 1\rangle$, corresponding to the coherent exchange of a single photon between qubit and resonator. This can also be viewed as an exchange of one bit of quantum information (encoded in the resonator mode's Hilbert space spanned by the Fock states $|0\rangle$ and $|1\rangle$), which can then be transferred to another qubit coupled to the same resonator [18]. Achieving high fidelity in this transfer, however, requires extremely high Q for the resonator, since the photon spends at least a time of order the Rabi period stored inside it. To relax this requirement, most cQED is performed instead in the regime of large detuning $\Delta_q \gg g_\perp$, known as the dispersive limit, where the effective coupling, to second order in $\hat{H}_\perp$, is $\approx g_\perp^2/\Delta_q$. Although $g_\perp$ must be made larger by a factor $\Delta_q/g_\perp \gg 1$ compared to the resonant case to achieve the same operation speed, the time spent by the photon in the resonator is effectively reduced to Δ_q^{-1}; this can be viewed as virtual photon exchange, in the sense that the photon moves to a different energy by entering the resonator, but only for a time consistent with the uncertainty principle. The detuning also provides a natural means of controlling the effective qubit–resonator interaction, since in most cases the transition dipole μ_q of the qubit is not dynamically adjustable, whereas its energy splitting $\hbar\omega_q$ often is[2].

This cQED paradigm has been extremely fruitful for quantum information processing (QIP), and has already been used to demonstrate many important QIP functions including complete multi-qubit algorithms [24, 25]. In some cases it is already the basis for envisioned scaling to much larger systems [26–28]. In spite of its great success in the QIP area, however, cQED also has some characteristic limitations when used in this context. For example, when a qubit is engineered to have a large transition dipole so that it can have strong $g_\perp$ for cQED, it necessarily becomes more sensitive to its electromagnetic environment (i.e. it can couple to spurious environmental modes as well as the desired resonator mode) [29]. In addition, since cQED effectively uses quantum states of the resonator to store or transport quantum information, its protocols are quite sensitive to the presence of spurious photon populations in the resonator (including in some cases those in higher modes) which are often encountered in these experiments [30–32], and also to a lesser extent its quality factor Q. Next, although adjustment of the detuning Δ_q does provide effective control of the relevant interactions in experiments to date, it does not in general allow a very strong suppression of the coupling when it is intended to be off, since it scales only as $\sim 1/\Delta_q$; furthermore, the adjustability of the qubit energy required for this control necessarily implies that the qubits are sensitive to noise in whatever parameter is used for this adjustment (e.g. charge or flux noise, or noise in the external bias itself) [21–23]. Finally, since in the dispersive limit of cQED interaction with a

[2] An exception to this is [19], where the qubit's intrinsic electromagnetic coupling can be adjusted independently of the cavity. Also, an alternative method for achieving tunability is to keep the coupling to the cavity on with the detuning fixed at a large value, and use the resulting weak, static coupling in conjunction with a strong driving field [20–23].

qubit requires exchanging a virtual photon with it, direct N-qubit interactions get exponentially weaker as N increases. This implies that sequential, pairwise interaction between qubits will likely remain the best way to achieve N-qubit entanglement in cQED, even when all of the N qubits are coupled to the same resonator. In this case one must take care when scheduling the various ramps of the qubit energies, since whenever any two qubits come close to resonance with each other they must both be very far detuned from the resonator to avoid spurious entanglement.

In this paper, we describe an alternative approach for coupling qubits and electrical resonators via electromagnetic interactions, which does not involve any photon exchange between them, and therefore largely avoids these limitations. In contrast to the transverse interaction $\hat{H}_\perp$ of cQED (cf equation (2)), we will show how one can generically realize a 'longitudinal' interaction[3] of the form

$$\hat{H}_{||} \approx \hbar g_{||}(\hat{u}\hat{\sigma}_{\mathrm{q}}^{z}), \tag{3}$$

where $\hat{u} \equiv (\hat{a} + \hat{a}^\dagger)/\sqrt{2}$ is the dimensionless resonator coordinate. This interaction energy, being linearly proportional to the 'position' of the resonator, constitutes an effective force acting on it which depends on the qubit's internal state (via the operator $\hat{\sigma}_{\mathrm{q}}^{z}$). Our proposal is built on an analogy between this interaction and demonstrated methods [40, 41] developed by Mølmer and Sørensen [42, 43] and Milburn *et al*, [44] for entangling trapped atomic ions via qubit-state dependent forces acting on their collective center-of-mass vibrational modes (whose role is played here by the microwave resonator mode). In contrast to cQED as described above, our scheme involves only quasiclassical resonator states (whose quantum fluctuations can be small), under the influence of effectively classical, qubit-state-dependent forces[4]. As a result, the resonator dynamics which drive the gate operations are classical and macroscopic in nature, do not depend at all on the qubit frequency ω_{q}, and are insensitive to thermal or other fluctuations and damping. In addition, because the interaction does not rely on photon exchange, all of the qubits coupled to the same resonator can be entangled in the same amount of time it takes to entangle only two of them, and any subset of the qubits can be similarly entangled with negligible effects on the others.

In section 2 below, we describe the general qubit–resonator system under consideration. Section 3 contains a detailed description of how entangling operations can be achieved between qubits coupled to a common resonator, without any real or virtual exchange of photons. In section 4 we consider in detail the leading sources of error in two-qubit entangling operations, and evaluate these errors for a variety of different physical qubit modalities, which are tabulated in table 1. We conclude in section 5 with a summary of the differences between our proposal and cQED. Appendix A gives a comparison between our proposal and the analogous trapped-ion gates on which it is based, appendices B and C describe certain aspects of the

[3] Qubit–resonator or qubit–qubit couplings with longitudinal character have been considered previously in various forms: in [33–35] for superconducting charge qubits, in [36–38] for superconducting flux qubits, and in [39] as a way to measure geometric phases of a resonator.

[4] Qubit-state-dependent resonator displacements can also be realized in the dispersive limit of cQED by driving the resonator and using the qubit-induced dispersive frequency shift of the resonator to achieve a state-dependent result. In [45, 46] this effect was used for manipulation or measurement of a resonator state by a single qubit. This is distinct from our proposal, in that it involves virtual exchange of photons and can be viewed as a nonlinear response of the system to a resonator drive. By contrast, in the present work the force on the resonator is explicitly qubit-state-dependent, the system remains linear, and only the qubits are driven.

Table 1. Selected examples of two-qubit controlled-π gate parameters (details for each system are contained in appendix D). For transmission-line resonators, L_r and C_r are effective values for a given longitudinal mode. The results for gate errors shown are the thermal photon-number dephasing rate Γ_ϕ (equation (25)) (which is present due to the coupling even when no two-qubit gates are being driven), the gate time t_π (equation (19)), the state-dependent displacement error $\epsilon_{\delta\alpha}$ (equation (21)) and the resonator fluctuation error $\epsilon_{\delta\eta^+}$ (equation (24)). The total two-qubit error is defined as: $\epsilon_{2qb} \equiv 2\Gamma_\phi t_\pi + \epsilon_{\delta\alpha} + \epsilon_{\delta\eta^+}$. This does not include single-qubit errors unrelated to the coupling (e.g. T_1 relaxation for the superconducting qubits or charge-noise dephasing for the quantum dots). The quantity Δ_{hm} is the minimum detuning to the next higher oscillator mode (assuming it has the same Lamb–Dicke parameter as the fundamental), such that the associated error $\epsilon_{hm} \leqslant 0.1 \times \epsilon_{2qb}$ (equation (C.1)). In all cases we take a resonator temperature of $T_r = 40\,\mathrm{mK}$, corresponding to $\bar{n} = 0.4, 0.03, 4 \times 10^{-6}, 10^{-8}$ for $\omega_r/2\pi = 1, 3, 10, 15\,\mathrm{GHz}$. Note that both donor spins in Si and NV centers in diamond do not themselves require low temperatures, but here they are required to suppress errors due to classical, thermal resonator fluctuations (cf equations (24) and (25)).

Qubit type	Q	$\omega_r/2\pi$ (GHz)	L_r (pH)	C_r (pF)	η_0^- ($\times 10^3$)	δ_m($\times 10^3$)	m
Flux	25000	10	250	0.84	4.5	64	100
[57, 58]	10^6	10	500	0.46	3.4	12	6
	10^6	1	30 nH	0.84	1.4	2.9	2
Transmon	50000	10	250	0.84	1.4	14	50
[73]	10^6	10	250	0.84	1.4	6.2	10
	10^6	3	1500	1.8	1.1	2.2	2
S-T QDs	25000	15	100 nH[a]	1.1 fF	3.0	33	60
[60–63]	10^6	15	30 nH[a]	3.7 fF	1.7	6.6	8
$CaCl^+$ [3]	10^6	1	1000 nH[a]	25 fF	0.14	1.1	30
^{31}P–^{28}Si [64]	10^7	1	100[b]	250	0.014	0.14	50
NV [65]	10^7	1	100[b]	250	0.028	0.13	10

Qubit type	Γ_ϕ^{-1} (ms)	t_π (ns)	$\epsilon_{\delta\alpha}$ ($\times 10^3$)	$\epsilon_{\delta\eta^+}$ ($\times 10^3$)	ϵ_{2qb} ($\times 10^3$)	Δ_{hm} (GHz)	N_γ
Flux	8.4	160	0.015	2.0	2.0	2.3	2600
[57, 58]	0.76	51	10^{-9}	0.27	0.34	3.5	5200
	0.23	700	2×10^{-8}	2.0	5.0	0.03	3.1×10^6
Transmon	126	360	0.053	4.5	4.6	0.4	10^4
[73]	6.3	160	7×10^{-8}	0.51	0.53	0.9	10^4
	0.10	300	3×10^{-8}	1.5	4.5	0.07	2.0×10^5
S-T QDs	3.0	120	0.20	3.8	4.0	1.4	2.5
[60–63]	0.83	80	5×10^{-7}	0.47	0.57	1.4	8.5
$CaCl^+$ [3]	25s	27μs	0.0032	5.1	5.1	0.01	2.4×10^9
^{31}P–^{28}Si [64]	2×10^7s	350μs	0.005	4.0	4.0	0.5 MHz	2.4×10^9
NV [65]	2s	78μs	6×10^{-5}	4.4	4.5	0.8 MHz	2.4×10^9

[a] Impedances this high require the use of high-kinetic-inductance materials [29, 74–78]. Limits on achievable resonator Q and impedance for these materials are as yet unknown.
[b] Impedances this low may not be achievable in a transmission-line resonator.

gate error calculations, and appendix D concerns the assumptions and parameter values used to evaluate the gate errors shown in table 1.

2. General qubit–resonator system

We first consider a single qubit coupled to a microwave resonator, using the circuits of figures 1(a) and (b) to describe capacitive and inductive qubit/resonator coupling, respectively. These two circuits are chosen to be exactly *dual* [47–52] to each other, so that they are governed by equations of identical form, and the solution for one case can be mapped directly to the other using the transformation: $Q \leftrightarrow \Phi$, $C \leftrightarrow L$, $V \leftrightarrow I$, $Y \leftrightarrow Z$. In each of these circuits, the qubit is described by the eigenenergies $E_{\rm q}^{g}(p)$ and $E_{\rm q}^{e}(p)$ of its energy eigenstates $|g\rangle$ and $|e\rangle$, respectively, which are assumed to be functions of a parameter p

$$\begin{aligned}\hat{H}_{\rm q} &\equiv E_{\rm q}^{g}(p)|g\rangle\langle g| + E_{\rm q}^{e}(p)|e\rangle\langle e| \\ &= \tfrac{1}{2}[E_{\rm q}^{+}(p)\hat{I} + E_{\rm q}^{-}(p)\hat{\sigma}_{\rm q}^{z}],\end{aligned} \tag{4}$$

where $E_{\rm q}^{\pm}(p) \equiv E_{\rm q}^{e}(p) \pm E_{\rm q}^{g}(p)$ and $\hat{I}, \hat{\sigma}_{\rm q}^{z}$ are Pauli operators in the qubit Hilbert space. In figure 1(a), we have $p \to Q_{\rm q}$, which can be viewed as an induced offset charge bias for the qubit; in figure 1(b) we have $p \to \Phi_{\rm q}$, which can be viewed as an external flux bias for the qubit. Figure 1(c) shows schematically energies $E_{\rm q}(Q_{\rm q})$ applicable to the circuit of figure 1(a) by solid red and blue lines for the qubit states $|g\rangle$ and $|e\rangle$, respectively. Note that we focus here on the case where equation (4) holds even when p is time-dependent, so that $E_{\rm q}^{g}(p)$ and $E_{\rm q}^{e}(p)$ can be treated as classical potential energies in the context of the resonator dynamics. In this situation, any interaction with the qubit involving only the variable p cannot induce transitions between $|g\rangle$ and $|e\rangle$ and therefore cannot involve any photon exchange, and can have no transverse (dispersive) character of the form of equation (2).[5] In this case, as illustrated in (c) and discussed in detail below, the dynamical electrical properties of the qubits (for small excursions of p about a quasistatic bias point) can be described using the linear circuit elements shown in the shaded ovals.

The qubit–resonator interaction of interest here is represented generically by the coupling elements $C_{\rm c}$ and $L_{\rm c}$ in figures 1(a) and (b), respectively, which looking out from the resonator form a capacitive (a) or inductive (b) divider with the qubit. When the qubit/resonator coupling is zero (i.e. $C_{\rm c}$ in (a) replaced by an open or $L_{\rm c}$ in (b) replaced by a short), p is determined only by the external bias of the qubit ($V_{\rm b}$ or $I_{\rm b}$); for finite coupling, however, p acquires a contribution proportional to the resonator field. Figure 2 shows schematically a number of implementations of the proposed coupling, for different physical qubit modalities, which can be described by one or the other of figure 1(a) and (b) (see appendix D for details). For the superconducting qubit examples of figures 2(a) (transmon [10–13]) and 2(b) (flux qubit [57–59]) which have both been demonstrated extensively in a cQED architecture, we also show a direct comparison between

[5] In the case when $E_{\rm q}(p)$ are only *adiabatic* eigenenergies, and $|e\rangle$–$|g\rangle$ transitions can be driven by time-dependent p via nonadiabatic effects, a nonzero transverse interaction is present. The coupling scheme we discuss in this work can still be used in this case as long as the transverse component of the interaction is made sufficiently small by, for example, using large $\Delta_{\rm q}$.

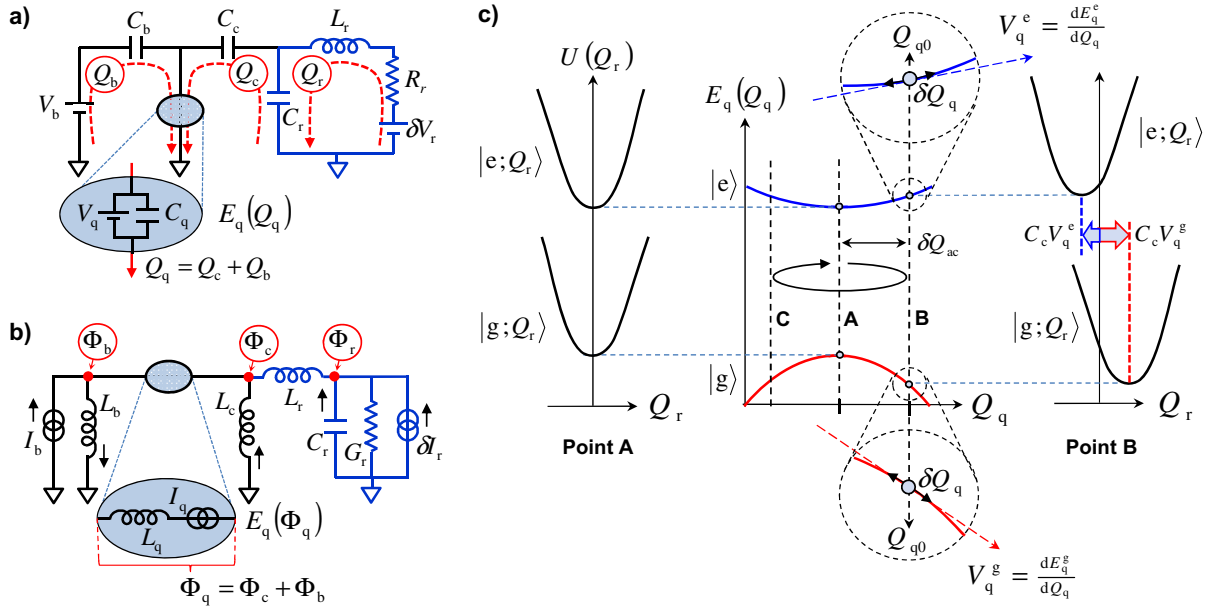

Figure 1. Electromagnetic qubit/resonator coupling without exchange of photons. (a) shows the electric circuit analyzed in detail; (b) is its exact dual [47–52], governed by equations of identical form. The resonator in both cases is indicated in the circuit schematic by a blue color; its damping, and the associated fluctuations, are modeled in (a) via R_r and the Langevin noise source δV_r, and in (b) by G_r and δI_r. In (a), the canonical coordinates of the circuit Q_b, Q_c, Q_r are known as loop charges [53], each of which is associated with an irreducible loop of the circuit as illustrated by the dashed red lines. The circuit of (b) is described using a dual representation in terms of the node flux variables Φ_b, Φ_c, Φ_r indicated by the red dots, whose sign relative to ground is defined by the branch orientations shown with black arrows. The qubit in each case is indicated by a shaded oval, and is described in our model by its eigenenergies $E_\mathrm{q}(p)$, with $p \in Q_\mathrm{q}, \Phi_\mathrm{q}$, which function as effective potentials to which the resonator is coupled. An example of these energies and their dependence on p is shown in (c) for the electric case $p \to Q_\mathrm{q}$ by red and blue lines for $|g\rangle$ and $|e\rangle$, respectively. In equation (6), we expand $E_\mathrm{q}(Q_\mathrm{q})$ in excursions δQ_q about a quasistatic bias point $Q_{\mathrm{q}0}$, as illustrated in (c). This expansion can be described by the circuit elements in the shaded oval of (a): the linear slope $\mathrm{d}E_\mathrm{q}/\mathrm{d}Q_\mathrm{q}$ is the voltage across the qubit, and the curvature $\mathrm{d}^2E_\mathrm{q}/\mathrm{d}Q_\mathrm{q}^2$ is the inverse of its effective capacitance C_q^{-1}. The former is the basis of our proposal for multiqubit gates, and results in an effective force on the resonator which displaces its equilibrium position by a (qubit-state-dependent) amount $C_\mathrm{c}V_\mathrm{q}$ (cf equation (7)), as illustrated in (c) for two different qubit bias points A and B. At point A we have $V_\mathrm{q}^{e,g} = 0$, and there is no force or displacement, while B illustrates the nonzero case. Dual statements to these can be made about the inductive case shown in (b). In our proposed gate operations, we modulate the force by modulating the qubit bias point, an example of which is illustrated in (c) by the curved arrow

Figure 1. (Continued) going from $A \to B \to C \to A$, and so on. Note that the effect of the second order term associated with C_q^{-1} (or its dual, inductive analogue) has previously been exploited as the basis for qubit–resonator interactions [54–56], but in the context of our proposal it contributes only a higher-order source of potential errors which we address in section 4 below.

that case which uses a transverse coupling of the form of equation (2), and our proposal, which has no transverse coupling and can be described by equation (3)[6].

To analyze our proposed qubit/resonator coupling in detail, we consider specifically the capacitively coupled circuit of figure 1(a) for definiteness, since the corresponding results for the inductive circuit of 1(b) can then be obtained using a duality transformation [47–52]. We write its classical potential energy in terms of the loop charges Q_b, Q_c, Q_r shown in the figure by dashed red lines (for the moment taking the damping resistance R_r and associated noise fluctuations δV_r to be zero), which play the role of canonical position variables in a Lagrangian description of the circuit [53]

$$U(Q_r, Q_c, Q_b) = E_q(0) + \frac{(Q_r - Q_c)^2}{2C_r} + \frac{Q_c^2}{2C_c} + \frac{Q_b^2}{2C_b} + \underbrace{\int_0^{Q_q} V_q(Q_q')\,dQ_q'}_{E_q(Q_q)-E_q(0)} - \int_0^{Q_b} V_b(Q_b')\,dQ_b', \tag{5}$$

where $Q_q \equiv Q_b + Q_c$, $V_q(Q_q) \equiv dE_q/dQ_q$ is the voltage across the qubit, $V_b(Q_b)$ is defined as the bias voltage for which the source has supplied a charge Q_b. The last two terms are the potential energies of the qubit and the source, respectively, and can be viewed as work done by (or on) the source as V_b is turned up from zero. Note that the magnetic circuit of figure 1(b) is described correspondingly in a dual representation where node fluxes play the role of position variables [53].

We now seek to expand equation (5) in deviations of the charges Q_n ($n \in b, c, r$) about their minimum-energy, quasistatic solutions Q_{n0}, which are given formally by: $Q_{b0} = C_b(V_b - V_q)$, $Q_{c0} = -C_c V_q$, $Q_{r0} = Q_{c0}$ (these solutions must be obtained self-consistently since V_q depends implicitly on Q_q). We now expand the qubit energy about this bias point, writing: $Q_n \equiv Q_{n0} + \delta Q_n$:

$$E_q(Q_{q0} + \delta Q_q) \approx E_q(Q_{q0}) + V_q \delta Q_q + \frac{\delta Q_q^2}{2C_q} + \cdots, \tag{6}$$

where the linear term is proportional to the qubit voltage V_q, and the quadratic term can be written in terms of an effective dynamic capacitance of the qubit $C_q \equiv (d^2E_q/dQ_q^2)^{-1}$ (also known as 'quantum capacitance' [54–56]), both of which are evaluated at Q_{q0}. As illustrated in figure 1(a), this expansion allows us to view the potential energy of the qubit in a circuit context

[6] Note that in figure 1(b) an inductive divider is used to couple the qubit to the resonator, rather than mutual inductances shown in the examples of figures 2(a) and (b); this allows us to retain an exact duality with the capacitive circuit of figure 1(a) so that our results can be applied to both cases. The use of mutual inductances can be accounted for with minor modifications to the results presented here.

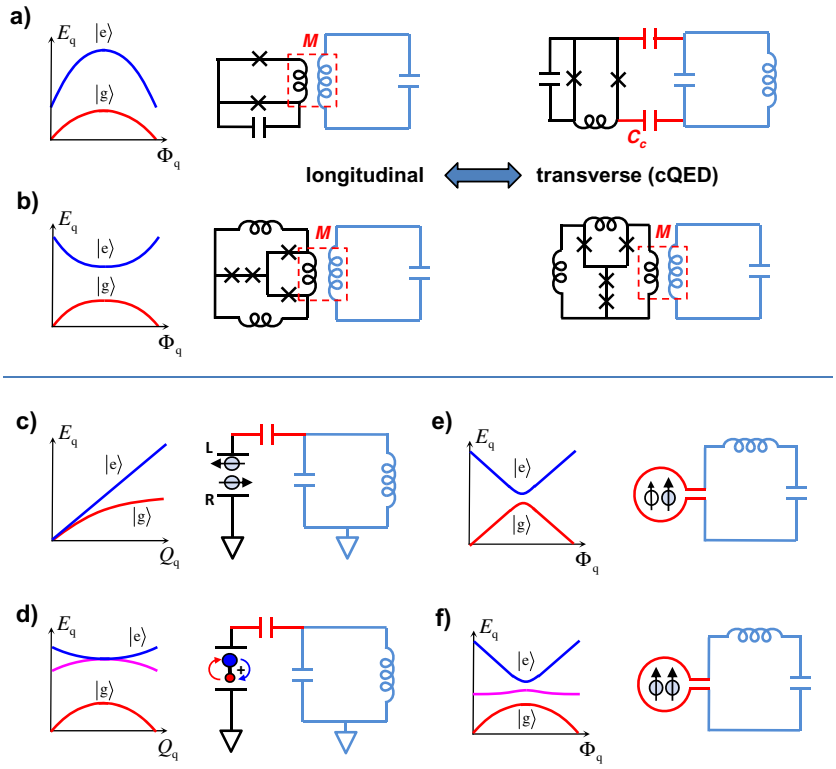

Figure 2. Examples of physical qubits coupled to resonators in the manner of our proposal. For each case we show a schematic of the equivalent circuit with the qubit in black, resonator in light blue, and the coupling element in red (note that the qubit bias connections are not shown). Next to each case are the corresponding energies $E_{\mathrm{q}}^{g}(p)$ and $E_{\mathrm{q}}^{e}(p)$ (see appendix D for details). Panels (a) and (b) are the transmon [10–13] and flux qubit [57–59], respectively, both of which have been extensively demonstrated in a cQED architecture. The left side of these panels shows our proposed longitudinal coupling for these cases, which can be described by the circuit of figure 1(b). The corresponding cQED circuits for these same qubits are shown for comparison on the right side of these panels. The inductors inside the qubits represent the usual geometrical loop inductances, which are typically neglected since they are much smaller than the Josephson inductances of the JJs. They are shown here only to illustrate mutual inductive coupling between qubit and resonator. Panels (c)–(f) show how our scheme can also be applied to a number of other qubit modalities: (c) singlet–triplet double quantum dot [60–63]; (d) polar molecular ion [3], where the third curve (shown in magenta) corresponds to the two degenerate $J = 1, m_{\mathrm{J}} = \pm 1$ levels; (e) ^{31}P coupled electron and nuclear spins in ^{28}Si [64], where we show only one nuclear spin orientation. The splitting at zero field is due to hyperfine coupling; and (f) nitrogen-vacancy center in diamond [65], with a fixed transverse magnetic field, as a function of an additional longitudinal field. The third (magenta) curve shows the two degenerate levels which become $m_{\mathrm{S}} = 0$ in the limit of large longitudinal field.

(for small excursions about Q_{q0}) as a voltage source V_q in parallel with the capacitance C_q (in the dual magnetic case of figure 1(b) this becomes a series current source I_q and inductance L_q). We emphasize that V_q and C_q depend on both the internal state of the qubit, and its bias Q_{q0}, though we have suppressed explicit notation of this dependence for clarity.

Of the three δQ_n, only δQ_r is an independent dynamical variable, since it couples to an inductance (the effective 'mass' for a fictitious particle whose 'position' is δQ_r [51–53]), while δQ_b and δQ_c are deterministically related to δQ_r. To determine these relations, we hold V_b and δQ_r fixed and minimize U with respect to δQ_c and δQ_b, to obtain: $\delta Q_b = 0$ and $\delta Q_r/C_r = \delta Q_c(C_r^{-1} + C_c^{-1} + C_q^{-1})$. Combining this with equations (5) and (6), integrating by parts, and re-expressing the result in terms of Q_r, we find

$$U(Q_r) = E_q(Q_{q0}) + \frac{(Q_r + C_c V_q)^2}{2C_r'}, \tag{7}$$

where we have defined the quantities

$$\begin{aligned} C_r' &\equiv C_r + \frac{C_c C_q}{C_c + C_q}, \\ \omega_r &\equiv \frac{1}{\sqrt{L_r C_r'}}, \quad Y_r \equiv \sqrt{\frac{C_r'}{L_r}} = \frac{1}{Z_r}. \end{aligned} \tag{8}$$

The quantity C_r' is the effective total capacitance of the resonator, which is just C_r in parallel with the series combination C_c and C_q as can be seen from figure 1(a) (C_b does not contribute to this because the qubit voltage is fixed at V_q independent of the resonator voltage, so that no charge is induced on C_b by small signals on the resonator). Note that when $C_c \to 0$, equations (7) and (8) reduce to the sum of the uncoupled qubit and resonator potential energies as expected. Also, as required by the total energy conservation expressed in equation (5), the classical potential energy of the coupled system at the resonator's equilibrium position is simply $E_q(Q_{q0})$, independent of the qubit bias point Q_{q0}.

From equations (7) and (8) we see that the leading-order effect of the coupling can be viewed as a displacement of the resonator mode's equilibrium 'position' by a qubit-state-dependent amount $C_c V_q$, as illustrated in figure 1(c). This displacement can be associated with an effective 'force' $V_q C_c/C_r'$ exerted by the qubit on the oscillator (as described by equation (3) above), whose 'spring constant' is $1/C_r'$. The next order effect arises from the qubit's dynamic capacitance C_q [54–56], which is in general qubit-state-dependent, and can therefore induce small state-dependent shifts in the resonator's frequency and impedance according to equations (8); these shifts can be a potential source of gate errors, as we discuss in detail below in section 4.

3. Controlled-phase gate with quasiclassical forces

The form of equation (7) and its interpretation in terms of a qubit state-dependent force on the resonator suggests an analogy with techniques developed for trapped atomic ions, in which state-dependent light forces acting on the atomic center-of-mass motion (analogous to the resonator in our case) produce entangling operations on the internal states of the atoms. We now show how similar entangling gates can be implemented in our system based on this analogy

(discussed in more detail in appendix A). Following [40–44], we describe the oscillator in terms of a dimensionless classical field amplitude[7]: $\alpha = \langle \hat{u} + \mathrm{i}\hat{v} \rangle$, where

$$\hat{u} \equiv \frac{\hat{Q}_\mathrm{r}}{\sqrt{\hbar Y_\mathrm{r}}} = \frac{\hat{a} + \hat{a}^\dagger}{\sqrt{2}},$$
$$\hat{v} \equiv \frac{\hat{\Phi}_\mathrm{r}}{\sqrt{\hbar Z_\mathrm{r}}} = \frac{\hat{a} - \hat{a}^\dagger}{\mathrm{i}\sqrt{2}} \tag{9}$$

and Φ_r is the canonical momentum of the oscillator such that $[\hat{u}, \hat{v}] = \mathrm{i}$. The quantity α is a c-number for a pure coherent state, while in the presence of thermal or other classical field fluctuations it can be written as a diagonal density matrix (e.g. using the Glauber–Sudarshan P-representation [17]). If we now include N qubits in our system which can be coupled to the resonator, in general all resonator and qubit quantities become operators in the 2^N-dimensional qubit Hilbert space, which henceforth we indicate with the usual caret operator notation: $\alpha \to \hat{\alpha}$, $\omega_\mathrm{r} \to \hat{\omega}_\mathrm{r}$, $Z_\mathrm{r} \to \hat{Z}_\mathrm{r}$, $Y_\mathrm{r} \to \hat{Y}_\mathrm{r}$, $E_\mathrm{q} \to \hat{E}_\mathrm{q}$, $V_\mathrm{q} \to \hat{V}_\mathrm{q}$, $C_\mathrm{q}^{-1} \to \hat{C}_\mathrm{q}^{-1}$). However, in the case of interest to us here, where equation (4) holds (i.e. there is no transverse coupling), all of these operators are *diagonal* in the qubit Hilbert space (and commute with the individual qubit Hamiltonians).

For our gate operations, we will exploit the qubit-state-dependent classical dynamics of the resonator, described by the operator $\hat{\alpha}$, while the qubit state dependences of $\hat{\omega}_\mathrm{r}$ and $\hat{Z}_\mathrm{r}$ implied by equation (8) are higher-order effects which we will consider as perturbations only, in section 4. To that end, we separate out the latter explicitly with the notation

$$\hat{\omega}_\mathrm{r} \equiv \tilde{\omega}_\mathrm{r}(1 + \delta\hat{\omega}_\mathrm{r}),$$
$$\hat{Z}_\mathrm{r} \equiv \tilde{Z}_\mathrm{r}(1 + \delta\hat{Z}_\mathrm{r}), \tag{10}$$

where the tilde is defined by: $\tilde{X}_\mathrm{r} \equiv \mathrm{Tr}[\rho_\mathrm{m}\hat{X}_\mathrm{r}]$, with $\rho_\mathrm{m} \equiv \hat{I}_{2^N}/2^N$ the completely mixed state of the N qubits, and $\hat{I}_d$ is the d-dimensional identity matrix. This definition separates the *average* qubit-induced renormalization of the resonator frequency and impedance from the small qubit-state-dependent corrections to this which we will consider as potential sources of error in section 4. We can now write the equation of motion for the oscillator with quality factor Q as [8]

$$\frac{\mathrm{d}\hat{\alpha}}{\mathrm{d}\tau} = -\mathrm{i}(1 + \delta\hat{\omega}_\mathrm{r})[\hat{\alpha} - \hat{\eta}] - \frac{\hat{\alpha} - \hat{\alpha}^*}{2Q}, \tag{11}$$

where $\tau \equiv \tilde{\omega}_\mathrm{r} t$, we have made the following replacements in equations (9) above: $Z_\mathrm{r} = 1/Y_\mathrm{r} \to \tilde{Z}_\mathrm{r} = 1/\tilde{Y}_\mathrm{r}$, and the dimensionless, qubit-state-dependent force $\hat{\eta}$ and frequency shift $\delta\hat{\omega}_\mathrm{r}$

[7] As long as equation (4) holds, a purely classical treatment of the resonator field is valid without approximation (provided, of course, that the resonator's initial state is itself classical).

[8] Equation (11) fully describes the classical dynamics of interest here as long as the qubit-induced effective force on the resonator is linear (i.e. our truncation to second order of the expansion of equation (6) is valid). Third and higher-order terms in E_q produce a purely classical nonlinearity, which is negligible in the cases considered here. For comparison, in cQED the breakdown of the linear dispersive approximation and the onset of the Jaynes–Cummings nonlinearity become important as the resonator drive is increased [66].

can be written

$$\begin{aligned}\hat{\eta} &\equiv \sum_{i=1}^{N}[(\eta^- + \delta\eta^-)\hat{\sigma}_i^z + (\eta^+ + \delta\eta^+)\hat{I}_i],\\ \delta\hat{\omega}_\mathrm{r} &\equiv \sum_{i=1}^{N}\delta\omega_\mathrm{r}^-\hat{\sigma}_i^z,\end{aligned} \tag{12}$$

where $i \in 1 \ldots N$ indexes the qubits, $\hat{\sigma}_i^z$ and $\hat{I}_i$ are the Pauli-z and identity operator for qubit i, and

$$\begin{aligned}\eta^\pm &\approx \frac{C_\mathrm{c}V_\mathrm{q}^\pm}{2\sqrt{\hbar\tilde{Y}_\mathrm{r}}},\\ \delta\omega_\mathrm{r}^- &\approx \frac{\beta_\mathrm{r}\beta_\mathrm{q}^-}{4},\\ \beta_\mathrm{r} &\equiv \frac{C_\mathrm{c}}{C_\mathrm{c}+C_\mathrm{r}}, \quad \hat{\beta}_\mathrm{q} \equiv \frac{C_\mathrm{c}}{C_\mathrm{c}+\hat{C}_\mathrm{q}}\end{aligned} \tag{13}$$

using the notation $X^\pm \equiv [\langle e|\hat{X}|e\rangle \pm \langle g|\hat{X}|g\rangle]$ with $\hat{X}$ a single-qubit operator. For the sake of clarity we have assumed all N qubits and coupling elements are identical (though the method we propose does not require this), and we have retained only the leading-order term in $\delta\omega_\mathrm{r}^- \ll 1$ (we will see in table 1 below that this is a very good approximation). Note that there is no nonzero $\delta\omega_\mathrm{r}^+$ because of our definition of $\tilde{\omega}_\mathrm{r}$ (cf equation (10)). The quantities $\delta\eta^\pm$ are Langevin noise terms, with $\delta\eta^-$ due to qubit bias noise, and $\delta\eta^+$ associated with the finite resonator Q. In our model (figure 1a) the latter comes from the Johnson–Nyquist noise δV_r of the resistance R_r ($Q = Z_\mathrm{r}/R_\mathrm{r}$). The resulting dimensionless noise power spectral density of the fluctuating force $\delta\eta^+$ can be written

$$\begin{aligned}S_{\delta\eta^+}(\Omega) &= \frac{C_\mathrm{r}^2\tilde{\omega}_\mathrm{r}}{\hbar\tilde{Y}_\mathrm{r}}\langle\delta V_\mathrm{r}(t)\delta V_\mathrm{r}(t')\rangle_\omega\\ &= \frac{2\Omega}{Q}\coth\left(\frac{\Omega\tau_\mathrm{c}}{2}\right),\end{aligned} \tag{14}$$

where the brackets denote an environment average, the subscript ω indicates a Fourier transform, $\Omega \equiv \omega/\tilde{\omega}_\mathrm{r}$ is dimensionless frequency and $\tau_\mathrm{c} \equiv \hbar\tilde{\omega}_\mathrm{r}/k_\mathrm{B}T_\mathrm{r}$ with T_r the effective resonator mode temperature.

To produce a gate which entangles a particular subset of the qubits coupled to a single resonator, we modulate the bias points of those qubits, as illustrated in figure 1(c), while leaving the other (bystander) qubits alone. This modulation results in an oscillatory force on the resonator $\hat{\eta} = \hat{\eta}_0\sin(\omega_\mathrm{m}t)$ which depends on the joint state of the qubits being modulated, and not on the state of the bystander qubits. Following the trapped-ion case [40, 42, 43], we choose a modulation frequency ω_m close to resonance with a particular resonator mode, whose field (described by the classical, complex α) begins to follow a qubit-state-dependent path in its u, v phase space, as illustrated in figure 3. Each amplitude in the qubits' Hilbert space then begins to accrue a geometric phase associated with the phase-space area enclosed by the corresponding oscillator path: $\hat{\phi}_g = \mathrm{Im}[\oint\hat{\alpha}^*\mathrm{d}\hat{\alpha}]$ (recall that the operator notation here refers

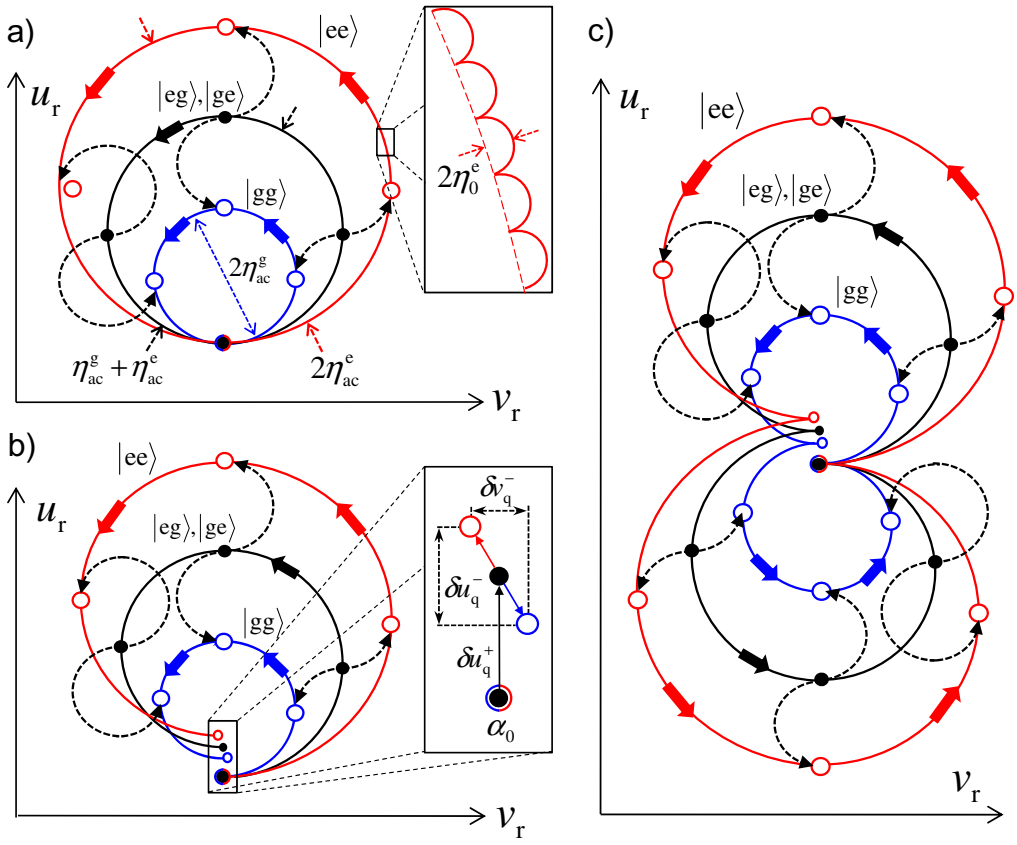

Figure 3. Oscillator phase space trajectories due to classical 'forces' exerted by two qubits. Trajectories are shown in a frame rotating at $\tilde{\omega}_r$, and the area enclosed within each path, indicated by solid lines ($|gg\rangle$—blue, $|eg\rangle$,$|ge\rangle$—black, $|ee\rangle$—red) is the geometric phase acquired by that amplitude of the qubits' internal-state wavefunction. Dashed arrows show the displacements of $|ee\rangle$ and $|gg\rangle$ *relative to* $|ge\rangle, |eg\rangle$, to make a connection between the general case considered here where $\langle eg|\hat{\eta}|eg\rangle, \langle ge|\hat{\eta}|ge\rangle \neq 0$, and the usual situation in the trapped-ion case $\langle eg|\hat{\eta}|eg\rangle, \langle ge|\hat{\eta}|ge\rangle = 0$ [40–43]. (a) In the ideal case ($Q \to \infty, \delta\hat{\omega}_r = 0$), the paths are closed. The inset shows the high-frequency component of the response due to the counter-rotating term in equation (15). (b) For finite $Q, \delta\hat{\omega}_r$, the trajectories are no longer closed, such that at the end of the gate a nonzero total oscillator displacement $\delta\alpha_q^-$ is entangled with the qubits' internal state. The inset shows the components $\delta u_q^{\pm}, \delta v_q^-$ of this residual displacement ($\delta v_q^+ = 0$ because $\delta\omega_r^+ = 0$); finite decay results in a shrinking radius of the path with time, producing finite δu_q^- at the end of the gate, and finite $\delta\hat{\omega}_r$ makes the modulation detuning δ_m weakly qubit-state-dependent, producing a nonzero δv_q^-. (c) modified gate sequence where either the force is reversed, or the qubits are inverted, in the middle of the gate, such that at the end of the gate the spurious entanglement between qubits and oscillator is removed.

only to the qubit Hilbert space; the resonator field is being treated as a classical, complex number in each dimension of this space). Neglecting for the moment the finite Q, fluctuations $\delta\eta^{\pm}$ and frequency shift $\delta\omega_{\mathrm{r}}^{-}$, and taking the modulation to be turned on at $\tau = 0$ with the oscillator in the state α_0 and not entangled with the qubit(s), we find (in a frame rotating at $\Omega_{\mathrm{m}} \equiv \omega_{\mathrm{m}}/\tilde{\omega}_{\mathrm{r}}$)

$$\hat{\alpha} = \hat{I}_N \alpha_0 \, e^{\mathrm{i}\delta_{\mathrm{m}}\tau} + \mathrm{i}\hat{\eta}_{\mathrm{ac}} \left[(\Omega_{\mathrm{m}} \, e^{\mathrm{i}\delta_{\mathrm{m}}\tau} - 1) - \frac{\delta_{\mathrm{m}}}{2} (e^{\mathrm{i}2\Omega_{\mathrm{m}}\tau} + 1) \right],$$
$$\hat{\eta}_{\mathrm{ac}} \equiv \frac{\hat{\eta}_0}{\delta_{\mathrm{m}}(2 + \delta_{\mathrm{m}})}, \tag{15}$$

where the detuning δ_{m} of the modulation is defined according to: $\omega_{\mathrm{m}} \equiv \tilde{\omega}_{\mathrm{r}}(1 + \delta_{\mathrm{m}})$.[9] In equation (15), the first term is free evolution, and the second and third terms can be viewed as the co- and counter-rotating components of the oscillator response, respectively, due to the effective force $\hat{\eta}_{\mathrm{ac}}$. These oscillator dynamics in phase space, for a two-qubit system, are illustrated in figure 3(a).

Note that the effective force $\hat{\eta}_{\mathrm{ac}}$ is inversely proportional to the detuning δ_{m} between the modulation frequency and the oscillator resonance, such that even if the resonator has additional internal modes, a single, desired mode can be selectively excited by tuning sufficiently close to resonance with it. We show in appendix C that this selectivity is more than sufficient to completely neglect spurious excitation of other modes in practical cases. It also allows multiple modes of the resonator to be used intentionally, in parallel, if they are reasonably well-separated and the resonator is linear. This makes it possible in principle both to perform entangling operations simultaneously on multiple, distinct subsets of the qubits coupled to a single resonator, or to perform much faster operations on a single subset of those qubits.

Qubit state-dependent forces necessarily result in entanglement between the qubits' internal states and the resonator mode field, as shown in figure 3 for the two-qubit case. Although this type of entanglement has interesting applications in its own right, in this work our goal is purely to entangle the qubits with each other, leaving no qubit–resonator entanglement (which could be a source of qubit decoherence) after the operation. Figure 3(a) illustrates how this can be achieved, following the atomic case [42–44]. The phase space trajectories of the oscillator are close to circular in the ideal case (due to a beating between the modulation-induced force and the resonant component of the oscillator's response to it) such that at certain times they all return to the initial point, and the entanglement of the oscillator with the qubits vanishes; if the modulation is turned off at one of these times, the net result is a state-dependent phase shift of the qubits only. The times τ at which this occurs are defined by the conditions

$$\frac{\delta_{\mathrm{m}}\tau}{2\pi} = m, \quad \frac{\tau}{2\pi} = \frac{k}{2}, \tag{16}$$

[9] It is also possible to simply turn a force on for a fixed time, with no oscillatory component. Such a scheme was considered for trapped ions in [67], and related methods for superconducting qubits were proposed in [33–35, 38]. Compared to our proposal, these techniques require much larger η to achieve the same gate speed (larger by a factor δ_{m}^{-1}), and they also provide no discrimination between the desired resonator mode and higher modes. In addition, they are sensitive to much lower noise frequencies near dc, as opposed to our scheme which is sensitive only to noise near the resonator frequency or its harmonics (as discussed in section 4).

where m, k are integers with $k > 2m$, and the resulting two-qubit state-dependent geometric phase is given by (neglecting overall phases):

$$\hat{\phi}_g = \frac{2\pi m}{\delta_{\rm m}^2(2+\delta_{\rm m})}[(\eta_0^-)^2\hat{\sigma}_1^z\hat{\sigma}_2^z + 2\eta_0^-\eta_0^+(\hat{\sigma}_1^z + \hat{\sigma}_2^z)]. \tag{17}$$

A controlled-π gate, sufficient in combination with single-qubit gates for universal quantum operations, is implemented (in addition to the single-qubit phase shifts given by the second term in equation (17), which one would need to correct using single-qubit rotations) if we choose

$$\eta_0^- = \delta_{\rm m}\sqrt{\frac{2+\delta_{\rm m}}{4m}} \tag{18}$$

in a total gate time τ_π (to leading order in $\delta_{\rm m}^{-1}$) of

$$\frac{\tau_\pi}{2\pi} \approx \sqrt{\frac{m}{2(\eta_0^-)^2}} \approx \frac{\delta_{\rm m}}{2(\eta_0^-)^2} \tag{19}$$

when equations (16) and (18) are satisfied.

Before discussing realistic errors in these operations in the next section, we highlight the qualitative distinction between the type of coupling we have been discussing and that used in cQED [10–13]. This can be compactly expressed by writing the effective coupling strength in both cases as the time-derivative of the two-qubit conditional phase (for our gates, the first term of equation (17))

$$\hbar\frac{{\rm d}\phi_{\rm c}}{{\rm d}t} \approx \begin{cases} \dfrac{\beta_{\rm r}^2}{2\delta_{\rm m}} \times \dfrac{1}{2}C_{\rm r}(V_{\rm q}^-)^2 & \text{this work,} \\ \dfrac{\beta_{\rm r}^2}{2\delta_{\rm q}} \times \hbar\omega_{\rm r}\dfrac{Z_{\rm r}}{R_{\rm q}} & \text{cQED,} \end{cases} \tag{20}$$

where in the latter case $\delta_{\rm q} \equiv \Delta_{\rm q}/\omega_{\rm r}$ is the dimensionless qubit–resonator detuning, and $R_{\rm q} \equiv h/4e^2$ is the superconducting resistance quantum. Notice that for our gate the energy scale of the effective interaction is purely classical and completely independent of the qubit frequency $\omega_{\rm q}$, since it is based only on deterministic, classical, driven resonator dynamics. By contrast, the cQED effective interaction energy is explicitly quantum, with the factor $Z_{\rm r}/R_{\rm q}$ describing zero-point fluctuations of the resonator ground state (inductive coupling in cQED would give the inverse of this factor, $R_{\rm q}/Z_{\rm r}$), and it depends explicitly on the detuning between qubit and resonator $\Delta_{\rm q}$. These features are a natural consequence of virtual photon exchange between qubit and resonator driven by vacuum fluctuations.

Because of this strongly quantum nature of the interaction in cQED, any classical fluctuations of the resonator must be negligible compared to its zero-point quantum fluctuations if high-fidelity operations are to be performed. As described in [30], the passage of a single spurious photon through any strongly coupled resonator mode during a quantum operation effectively makes a projective measurement of all the qubits coupled to it. Such fluctuations of the resonator are the inevitable result of photon exchange with transmission lines [30, 32] and qubits [68, 69] to which it is coupled, which often have a significantly higher effective temperature than the bath to which the experiment is nominally anchored. Thus, extremely careful filtering over a wide frequency range is necessary to suppress these fluctuation-induced errors in cQED [30]. By contrast, we will show that for our gates resonator fluctuations have only a higher-order effect, and only the specific mode near the modulation frequency contributes to this effect.

4. Two-qubit gate fidelity

In this section we evaluate sources of error in our two-qubit controlled phase gate. The results obtained in this section are tabulated in table 1 for a number of different physical qubit modalities and parameter assumptions. We begin with the effect illustrated in figure 3(b), spurious entanglement between qubits and resonator at the end of the gate in the form of a residual qubit-state-dependent oscillator displacement $\delta\alpha_{\rm q}^-$. The two mechanisms which produce this type of entanglement are finite resonator Q, and the state-dependent frequency shift $\delta\hat{\omega}_{\rm r}$ (induced by a state-dependent $C_{\rm q}$ or $L_{\rm q}$). As shown in figure 3(b), resonator decay causes the radius of the phase-space trajectory to shrink with time, while $\delta\hat{\omega}_{\rm r}$ effectively produces a detuning $\delta_{\rm m}$ (and corresponding evolution rate around the paths in phase space) which is qubit-state-dependent. These result in the spurious displacements illustrated in the inset: $\delta u_{\rm q}^- \sim \mathcal{O}(1/Q)$ and $\delta v_{\rm q}^- \sim \mathcal{O}(\delta\omega_{\rm r}^-)$, respectively.

Since both of these displacements result from classical and deterministic dynamics, however, we can strongly suppress them using the scheme shown in figure 3(c). We divide the gate excitation into two periods of equal duration (*each* of which satisfies equations (16)), and we switch the sign of the effective force $\eta_{\rm ac}$ between these two periods (alternatively, one could insert π-pulses to invert the qubits instead). This simple procedure works like a spin-echo, in the sense that the classical modifications to the trajectories cancel out at the end of the operation, removing the leading terms of order $\sim\mathcal{O}(1/Q)$, $\mathcal{O}(\delta\omega_{\rm r}^-)$ in the final displacement. The resulting gate error is, to leading order in the small quantities $\delta_{\rm m}$, η_0^-, Q^{-1}, $\delta\omega_{\rm r}^-$ and $\bar{n}$ (see appendix B)

$$\epsilon_{\delta\alpha} \approx \frac{mx^4}{4}\left[1 + 2\bar{n} + 2m\left(\frac{2\pi\delta\omega_{\rm r}^-}{x}\right)^2\right], \tag{21}$$

where $x \equiv \pi/(Q\eta_0^-)$ and m includes both halves of the gate. As we show in table 1, the result is essentially negligible compared to other error sources for all of the cases considered.

The more important potential source of errors is fluctuations of the qubits or resonator, which can produce single-qubit dephasing and fluctuations of the controlled-phase imparted during the entangling operation. One example of this is noise local to the qubits themselves, such as the ubiquitous 1/f charge and flux noise encountered in superconducting circuits [70]. Such noise is particularly important for qubits that do not have a degeneracy point like that shown by point A in figure 1(c) (where $V_{\rm q}^- = 0$ or $I_{\rm q}^- = 0$) and are therefore sensitive to low noise frequencies (e.g. singlet–triplet quantum dots [60–63]). Dynamical decoupling techniques have been extensively developed to suppress this sensitivity [71, 72], the simplest example of which is the spin-echo [70]. In our gate of figure 3(c) this could be naturally implemented by replacing the reversal of the gate force $\eta_{\rm ac}$ in the middle of the controlled-π gate with a π-pulse on each qubit, exchanging the roles of $|g\rangle$ and $|e\rangle$ (similar to [63]). Since these errors are entirely independent of our proposed method, we will not discuss them further here.

Higher-frequency noise (i.e. fluctuations *during* the gates), however, is an important source of error which we now consider. Assuming small fluctuations $\delta\eta^{\pm}$ of the force about the desired values, the system will accrue an additional geometric phase

$$\delta\phi_g \approx 2\int\{\delta\eta^-[\eta^+(\hat{\sigma}_1^z + \hat{\sigma}_2^z) + \eta^-\hat{\sigma}_1^z\hat{\sigma}_2^z] + \delta\eta^+[\eta^-(\hat{\sigma}_1^z + \hat{\sigma}_2^z)]\}\,{\rm d}\tau, \tag{22}$$

where the three terms are: single- and two-qubit phase errors due to fluctuations of the state-dependent force (predominantly qubit bias noise), and single-qubit errors due to oscillator

fluctuations (qubit bias noise can also contribute to this if $V_q^+ \neq 0$ or $I_q^+ \neq 0$). The resulting contributions to the average error can then be expressed in terms of mean square phase fluctuation amplitudes of the form

$$\langle \delta\phi_g^2 \rangle \sim \int S_{\delta\eta^+}(\Omega)|\eta^-(\Omega)|^2 \mathrm{d}\Omega, \tag{23}$$

where $S_{\delta\eta^+}(\Omega)$ is a dimensionless noise power spectral density (of the fluctuations $\delta\eta^+$ corresponding to the third term in equation (22)), $\eta^-(\Omega)$ is the Fourier transform of the time-dependent gate force $\eta^-(\tau)$, which is a peaked function centered on Ω_m, of width $\sim(2\tau_\pi)^{-1}$ and amplitude $\sim\eta_0^-\tau_\pi$. Since the gate forces $\eta^\pm$ oscillate at the frequency ω_m, only noise which occurs at or near this high frequency (or to a lesser extent its harmonics) will produce errors [71, 72]. Because of this, in nearly all cases low-frequency qubit bias noise (e.g. $1/f$ charge or flux noise) can be ignored for our gates, allowing us to neglect the contributions of the fluctuations $\delta\eta^-$ associated with the first two terms in equation (22).

The dominant source of high frequency noise in our model is then the thermal oscillator noise, which appears in $\delta\eta^+$, and which can become quite important as the Q of the oscillator is reduced. Using equations (14) and (23), we obtain the average error (per qubit)

$$\epsilon_{\delta\eta^+} \sim \frac{\pi}{\sqrt{2m}\,Q\eta_0^-} \coth\frac{\tau_c}{2}. \tag{24}$$

These errors will tend to restrict how small the resonator mode Q can be[10]. Note, however, that fluctuations of other resonator modes can be neglected; as described in appendix C, even the driven excursions of higher modes are negligible (at the error rates of interest here) due to the spectroscopic selectivity associated with driving the system near a specific, chosen mode.

In addition to the geometric phase errors just discussed in the controlled-phase gate, thermal resonator fluctuations can also produce direct dephasing of the qubits even when there is no gate modulation, if $\delta\omega_r^-$ is nonzero. This occurs because a qubit-state-dependent frequency shift of the resonator can also be viewed as an effective qubit frequency splitting ω_q' that depends on the resonator photon number n: $\omega_q' = \omega_q + 2n\delta\omega_r^-$ [10, 11]. For a thermal photon number distribution at temperature T_r with mean photon number $\bar{n}$, each qubit then experiences dephasing at the rate [10, 11][11]

$$\Gamma_\phi \approx 16\tilde{\omega}_r\bar{n}\,Q(\delta\omega_r^-)^2. \tag{25}$$

Notice that this dephasing rate *increases* with increasing resonator Q, as the discrete resonator frequencies associated with different photon number states become more resolved [10, 11]. This will tend to restrict how large the resonator Q can be.

Using equations (21), (24) and (25), we list in table 1 the parameter values and resulting gate errors for a number of specific examples, chosen to illustrate the utility of our scheme over a range of physical qubit modalities, resonator Qs, resonance frequencies and thermal photon populations $\bar{n}$. Note that in some cases two-qubit error rates as low as 10^{-3} are still achievable with $\bar{n}$ as high as 0.4 (for a 1 GHz resonator at 40 mK) and Q as low as 25 000,

[10] Note that in the absence of transverse coupling, noise at ω_q does not induce the usual enhanced spontaneous decay (Purcell effect) encountered in circuit QED [73].

[11] By contrast, a *coherent* state in the resonator with a given mean photon number does not cause qubit decoherence in our system (as it would in cQED due to quantum fluctuations of n) since the corresponding classical dynamics on which our gate is based are deterministic and fully taken into account by our analysis.

showing the robustness of our technique against resonator fluctuations and decay. For state-of-the-art experimental values such as: $Q \sim 10^6$ [79] and $\bar{n} \sim 10^{-3}$ [32], even lower error rates $\sim 10^{-4}$ become accessible (provided of course that single-qubit errors unrelated to the operations considered here are not the limiting factor).

We note in this context that while very high resonator Qs of 10^6 or greater are at present difficult to achieve in planar geometries at the single-photon level required for cQED implementations, this difficulty is substantially reduced at higher resonator powers ($\sim 10^3$–10^4 photons) where parasitic, lossy defects become saturated [79]. Given that our proposed method is in principle not affected by a coherent initial resonator state, one might consider the prospect of intentionally driving the resonator to increase the effective Q for gate operations (note, however, that the thermal fluctuation errors discussed above associated with T_r would also result from a nonzero effective temperature of an additional drive field). The simplest way to accomplish this would be to drive the resonator *instead* of the qubits, and use the qubit/resonator coupling to accomplish the modulation of $\hat{\eta}$ for the gate. In table 1 we list the quantity N_γ, the resonator photon number required to produce by itself the full qubit bias swing (via its coupling to the qubits) assumed for each set of gate parameters. In most cases, these values are comparable to or larger than the $\sim 10^3$–10^4 photons typically necessary to saturate the resonator loss in current experiments [12].

5. Conclusion

We have described an alternative method for coupling qubits and resonators which is qualitatively distinct from the current circuit QED paradigm. Unlike cQED, in which real or virtual photon exchange between qubits and resonator mediates the interaction [10–13], our proposal is based on a first-order, *longitudinal* coupling which does not involve any photon exchange, and which relies on purely classical dynamics of the resonator. We have shown how this coupling can be understood as a qubit-state-dependent effective force acting on the resonator, in a manner analogous to that which has been engineered between the internal spin states and center-of-mass vibrational modes of trapped atomic ions [40–44]. Our method has some potentially advantageous features when compared with cQED: first, since no photons are exchanged between qubits and resonator, there is no Purcell effect [73] and the qubits' excited-state lifetimes are decoupled both from the qubit–resonator detuning, and from the resonator Q. In fact, our method does not require the qubits to have any nonzero transition dipole moment at all, which opens the possibility of qubit designs that are intrinsically decoupled and therefore potentially much longer-lived [29]. The lack of photon exchange also implies that the coupling is independent of qubit frequency, which allows all qubits that have a degeneracy point to be biased at that point, so that they can remain insensitive to low-frequency noise even during quantum operations. Limitations associated with using the detuning between qubits and cavities to control the couplings [26–28] are largely removed, in particular with regard to

[12] One disadvantage of this scheme is that by driving the resonator, all qubits connected to it would necessarily become entangled. In architectures where this would be a problem, an alternative method would be to drive the resonator with a separate, *resonant* drive (i.e. at $\tilde{\omega}_r$) to saturate its loss, while driving only the desired qubits at ω_m; to avoid spurious entanglement from the resonant drive in conjunction with a nonzero $\delta\omega_r^-$, one would need to invert the sign of this resonant drive in the middle of the gate, resulting in a classical 'echo' similar to the method discussed above and shown in figure 3(c).

on/off coupling ratios and to implementation of complex, highly interconnected, many-qubit systems. Next, unlike in cQED where gate operations are linearly sensitive to the presence of spurious photons in any resonator mode coupled to the qubits [10, 11, 30–32], our scheme is only sensitive to occupation of a single, spectroscopically selected resonator mode, in higher order, such that it can tolerate substantial thermal occupation of that mode (up to $\bar{n} = 0.4$ was considered in table 1) before significant errors occur. This mitigates the need for an extremely low effective resonator temperature and/or a high resonator frequency (i.e. $T_r \ll \hbar\omega_r/k_B$). Also, since a classical drive field in the resonator does not produce errors in our gates, it may even be possible to intentionally drive it into the regime where high Q is much easier to achieve than in the single-photon limit required for cQED [79]. Third, because our coupling scheme gives an effective interaction $\propto (\eta \sum_i \hat{\sigma}_i^z)^2$ [42, 43], its strength does not decrease as the number of interacting qubits increases, in principle enabling multiqubit interactions or joint measurements to be implemented directly [80]. By contrast, in cQED, multiqubit interactions must either be engineered by cascading or combining pairwise interactions [24, 25, 81–84] or using weaker, higher-order multiqubit couplings involving more than one virtual exchange of photons with the resonator. Multiqubit interactions may be of interest, for example, in cluster-state generation [85], quantum simulation of Fermionic systems [86], or syndrome extraction in quantum error-correction schemes such as surface codes [87] and low-density parity check codes [88]. Finally, our scheme can also be used as a QND readout technique: one simply modulates the qubit bias at the oscillator resonance, such that the field amplitude and/or phase to which the oscillator rings up depends on the state of the qubit. Such a readout has the important advantage that it does not suffer from the dressed dephasing effects encountered in conventional dispersive readout in cQED [89].

Acknowledgments

We acknowledge helpful discussions with and/or comments from Daniel Greenbaum, Archana Kamal, Arthur Kerman, Adrian Lupaşcu and William Oliver. This work is sponsored by the Assistant Secretary of Defense for Research and Engineering under Air Force Contract # FA8721-05-C-0002. Opinions, interpretations, conclusions and recommendations are those of the author and are not necessarily endorsed by the United States Government.

Note added in proof. An error-suppression method closely related to that shown in figure 3(c) was recently demonstrated for trapped atomic ions in Hayes *et al* (2012 *Phys. Rev. Lett.* **109** 020503).

Appendix A. Comparison with trapped-ion gates

In laser cooling and manipulation of trapped atomic ions, the internal states of the ions are coupled to their center-of-mass motion by the photon recoil momentum $\hbar k$ associated with the (state-dependent) absorption of a photon with wavevector k. This coupling occurs in one of two ways: (i) via Rayleigh scattering of laser photons tuned near resonance with an electronic transition from an incident laser wavevector $\mathbf{k}_L$ to $\mathbf{k}'$, which imparts a recoil momentum $\hbar(\mathbf{k}_L - \mathbf{k}')$ (radiation pressure) and can be used to implement dissipative laser cooling of the atomic motion [90]; or (ii) via coherent (stimulated) scattering far from resonance, also known

as the ac Stark shift or light shift, which can be used to realize essentially non-dissipative forces with internal-state-dependence [40, 41, 91]. Our proposal is the analogue of the latter case[13].

The method we have presented, although broadly similar to the so-called Mølmer–Sørensen [42, 43] and 'ZZ' gates [40] used for trapped ions, has some important and favorable differences from those gates. For example, in our proposal, the resonator modes are nearly (though not completely) independent of the qubits, so that adding more qubits does not generate additional nearby collective modes which must be avoided as in the case of trapped ions. Also, in the ion case the equivalent controlled-phase interaction requires the ions to be in magnetic field sensitive states (in order to be sensitive to the spin-dependent optical forces used for the gates), which produces inevitable dephasing [40]. By contrast, in our proposal, although the states used must also be field-sensitive for the resonator to experience the required forces, in many cases the sign of this sensitivity is oscillating at a high frequency, such that dephasing due to low-frequency noise will be strongly suppressed. See, for example, figure 1(c) where during a gate the qubit bias point would be oscillating symmetrically about the symmetry point marked A; for noise frequencies much smaller than the modulation frequency (which is ∼GHz for the examples considered here) the bias modulation will be averaged out, and the system will remain first-order insensitive to the noise. Put another way, the dominant noise sensitivity occurs only at the modulation frequency, and not near dc, as described by equation (23) (of course, this can only be the case for qubits with a field-insensitive symmetry point about which to modulate). Although alternative methods for ions have been demonstrated that use states without field sensitivity [41–43], they have additional complications which limit the gate speed, fidelity, and number of ions that can be entangled [42, 43]. Finally, although the schemes used for ions are nominally insensitive to the state of the resonator, they still require a small Lamb–Dicke parameter, meaning that the ions must be localized to a much smaller region than the laser wavelength to avoid sampling a spatially dependent force [42, 43]. This can be particularly challenging in the context of the ubiquitous heating observed in ion traps, which causes η to increase in time, in the absence of active laser cooling [93]. In our case, although η is also a small parameter (in the expansion of $E_q(p)$), this expansion does not break down as in the atomic case; in fact, most of the error sources we have discussed actually *decrease* with larger η. In the expansion of equation (6), we included terms up to second order in the resonator displacement δQ_r, and for the parameters in table 1 the errors associated with the second order term (cf equations (21) and (25)) are already small enough for low error rates, and the higher-order terms can almost always be neglected completely. One possible exception to this would be associated with the presence of a strong *quartic* term in the qubit energy; this results in a modulation of ω_r at *twice* the input modulation frequency, which then *parametrically* excites the oscillator. We have simulated this effect, and it is negligible for the parameters considered here, though it is possible it could become important in some cases.

Appendix B. Spurious state-dependent resonator displacements

We seek to estimate the gate error that results when a nonzero entanglement between qubit state and oscillator displacement $\delta\alpha_q^-$ remains at the end of the gate. We can bound this error using the fidelity [94] between the desired qubit density matrix after the gate ρ_f^{qb} and the trace over

[13] There is also an analogy with our system for case (i), which allows resolved-sideband cooling *of the resonator*. Sidebands of this kind have in fact been observed in a superconducting circuit in [92].

resonator states of the actual total density matrix after the gate $\rho_{\rm f}^{\rm tot}$ [14]:

$$\begin{aligned}
\epsilon_{\delta\alpha} &\approx 1 - \left(\mathrm{Tr}\left[\sqrt{(\rho_{\rm f}^{\rm qb})^{1/2}\mathrm{Tr}_{\rm r}[\rho_{\rm f}^{\rm tot}](\rho_{\rm f}^{\rm qb})^{1/2}}\right]\right)^2, \\
\rho_{\rm f}^{\rm tot} &\equiv D_{\rm q}^{\dagger}\left[\rho_f^{\rm qb} \otimes D^{\dagger}(\alpha_0+\delta\alpha_{\rm q}^{+})\rho_{\rm th}^{\rm r} D(\alpha_0+\delta\alpha_{\rm q}^{+})\right] D_{\rm q}, \\
D_{\rm q} &\equiv D\left[+\frac{\delta\alpha_{\rm q}^{-}}{2}\right]|gg\rangle\langle gg| + D\left[-\frac{\delta\alpha_{\rm q}^{-}}{2}\right]|ee\rangle\langle ee|,
\end{aligned} \tag{B.1}$$

where $\rho_{\rm th}^{\rm r}$ is a thermal resonator state with temperature $T_{\rm r}$, $D(\delta\alpha)$ is the displacement operator in u, v phase space for (complex) displacement $\delta\alpha$, and $D_{\rm q}$ performs the state dependent displacement shown in figure 3(b). As an approximate worst case estimate, we take: $\rho_{\rm f}^{\rm qb} = [|gg\rangle + |ee\rangle][\langle gg| + \langle \mathrm{ee}|]/2$, and find (using the results of [96])

$$\epsilon_{\delta\alpha} \approx \frac{|\delta\alpha_{\rm q}^{-}|^2}{4}(1+2\bar{n}) \tag{B.2}$$

to leading order in $\delta\alpha_{\rm q}^{-}$ and $\bar{n} \approx \exp(-\hbar\omega_{\rm r}/k_{\rm B}T_{\rm r})$, the mean thermal photon number in the resonator, and independent of $\alpha_0 + \delta\alpha_{\rm q}^{+}$.

To evaluate the displacement $\delta\alpha_{\rm q}^{-}$ due to nonzero resonator damping and finite $\delta\omega_{\rm r}^{-}$, we first renormalize the oscillator resonance frequency to account for the usual Q-induced shift

$$\tilde{\omega}_{\rm r} \to \tilde{\omega}_{\rm r}\sqrt{1-\frac{1}{4Q^2}} \tag{B.3}$$

and correspondingly renormalize the dimensionless time τ (equation (11)), modulation frequency $\omega_{\rm m}$, detuning $\delta_{\rm m}$ and the conditions for m and k (equation (16)). The result, obtained by integrating equation (11) analytically for the gate shown in figure 3(c) and expanding the result to leading order in the small quantities $\delta_{\rm m}$, η_0^{-}, Q^{-1}, $\delta\omega_{\rm r}^{-}$, is

$$|\delta\alpha_{\rm q}^{-}|^2 \approx mx^4\left[1+2m\left(\frac{2\pi\delta\omega_{\rm r}^{-}}{x}\right)^2\right], \tag{B.4}$$

where $x \equiv \pi/(Q\eta_0^{-})$ and m now includes both halves of the gate. Combination of equations (B.2) and (B.4) yields equation (21).

Appendix C. Spurious excitation of higher resonator modes

In the presence of the gate modulation force, higher modes in the resonator [31, 73] will necessarily also be displaced by interaction with the qubits, according to their effective capacitance (inductance for the magnetic case of figure 1(b)) and geometrical coupling factors. The resulting (state-dependent) excursions of these modes do not in general decouple from the qubit at the same time as the fundamental mode (cf figure 3), leaving a spurious entanglement between the qubits and the higher modes at the end of the gate. However, just as in the atomic case [42–44], the excursions of higher modes are suppressed by their detuning from

[14] By defining the error in this way, we are neglecting any long-term quantum coherence of the oscillator, and assuming that its coupling to the environment will produce decay to a statistical mixture of coherent states, the so-called 'pointer states' of the system [95].

the modulation, since the effective force in the rotating frame is inversely proportional to that detuning (cf equation (15)). Using equation (B.2) for the error due to a state dependent excursion $\delta\alpha_k^-$ of mode k with frequency $\omega_{r,k} \equiv f_k\omega_r$, and taking $\delta\alpha_k^-$ to be $\sim\eta_{ac,k}^-$ the effective Lamb–Dicke parameter for that mode (cf equation (15)), we obtain the following estimate for the error due to excitation of higher modes:

$$\epsilon_{hm} \sim \frac{(\eta_{0,k}^-)^2(1+2\bar{n})}{2\left(1-f_k^{-2}\right)^2}. \tag{C.1}$$

Using this result, we list in table 1 the minimum separation Δ_{hm} from the fundamental to the next higher mode, assuming that $\eta_{0,k}^- = \eta_0^-$, which would give rise to an error ϵ_{hm} *one tenth* of the total error from all other sources. In all cases $\Delta_{hm} < \omega_r$, indicating these errors are unlikely to be significant in practical cases.

One interesting possibility to consider in this context is that if the higher modes of the resonator are all commensurate with the fundamental (as is the case in an ideal transmission-line resonator), all of the higher modes will decouple from the qubits *at the same time* as the fundamental. Since the geometric phases of all modes add together, this means that one could in principle implement a much faster gate by exciting many modes simultaneously using a modulation waveform which contains higher harmonics. The complication with this idea for real systems is that the higher modes are never quite commensurate with the fundamental, for example due to the reactance of the input coupling elements. To make this work, one would then need an appropriately tailored modulation waveform which selectively excites only those higher modes that are close enough to commensurate with the fundamental to keep the resulting errors low.

Appendix D. Details on error estimates in table 1

D.1. Superconducting qubits

For the transmon qubit (figure 2(a)), we take $\omega_q(\Phi_{b0}=0)/2\pi = 15\,\text{GHz}$, which gives $L_q^- = L_q^+/2 = -2(\Phi_0/\pi)^2/\hbar\omega_q = -87.4$ nH. We assume a modulation excursion $\delta\Phi_{ac} = 0.2\Phi_0$, corresponding to $\omega_q(0.2\Phi_0) = 13.5\,\text{GHz}$. For the flux qubit (figure 2(b)), we take $E_J/h = 200\,\text{GHz}$, $E_C/h = 5.7\,\text{GHz}$, and $\alpha(\Phi_{b0}) = 0.74$. This gives $\omega_q(\Phi_{b0})/2\pi = 4.73\,\text{GHz}$ and $L_q^- = 15.9$ nH, $L_q^+ = 0$ [15]. We assume a modulation amplitude of $\delta\Phi_{ac} = 0.1\Phi_0$, corresponding to $\alpha(0.1\Phi_0) = 0.70$ and $\omega_q(0.1\Phi_0) = 7.8\,\text{GHz}$. For both flux and transmon qubits we take $L_c = 25\,\text{pH}$.[16] Also for both of these cases we must consider the effect of junction asymmetry in the dc SQUID (defined by the area asymmetry parameter: $A_J \equiv 2(A_1 - A_2)/(A_1 + A_2)$), which produces a spurious coupling between external flux and the SQUID plasma mode. For the limit $L_c \ll L_J$ satisfied here, we find the matrix element for the modulation to couple to the first excited vibrational state of the plasma mode: $M_A \approx (\delta\Phi_{ac}/\Phi_0)A_J\sqrt{\pi/4}\hbar\omega_q$. We then have a maximal probability in this excited state of $\sim(\pi/4)(\delta\Phi_{ac}/\Phi_0)^2A_J^2(\omega_q/(\omega_q-\omega_m))^2$. Thus, for $A_J < 0.05$ and $\delta\Phi_{ac} < 0.2\Phi_0$, this error is at the 10^{-4} level or below. This calculation also gives

[15] For the flux qubit calculations, we use the numerical methods described in [29].

[16] With dc SQUID junction capacitances of $C_J \sim 3$fF this gives a plasma frequency for the circulating mode of $1/2\pi\sqrt{L_cC_J/2} = 0.8$ THz, so that the driving considered here will negligibly excite it.

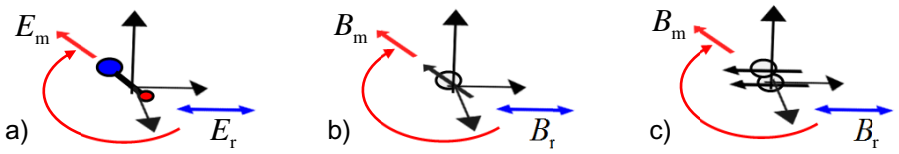

Figure D.1. Orientation of vector qubits driven by rotating fields. (a) Trapped molecular ion qubits, and (b) electron spin qubits driven by a rotating field E_m or B_m, respectively, whose rotation plane contains the resonator mode field direction; in both cases the dipole orientation follows the modulation field. In (c), the NV center spin triplet is driven by a rotating magnetic field B_m whose rotation plane contains the resonator mode field (B_r) direction; the orientation (quantization axis) of the NV center is determined by the crystal, and is also contained in the modulation field's rotation plane.

a residual, direct Jaynes–Cummings type coupling between dc SQUID plasma mode and the resonator: $g \approx \omega_q \beta_r A_J \sqrt{Z_r/8R_Q}$, which can be neglected in the cases considered here.

D.2. Singlet–triplet coupled quantum dots

Figure 2(c): The singlet–triplet coupled quantum dots (and molecular ions below) are biased with a voltage, rather than a charge, so that: $C_b, C_c \gg C_q$ (the opposite limit from the superconducting qubit cases). In this limit, the voltages across C_b, C_c can be neglected, and $V_q \approx V_b$. The quasicharge is then: $Q_q \approx dE^-/dV_q$ evaluated at V_b. The displacement of the resonator in equation (7) is then $C_q V_b$ and instead of equations (6) and (12), we have: $\eta_0^- \equiv (dE^-/dV_q)/(2\sqrt{\hbar Y_r})$, $C_q^- \equiv d^2E^-/dV_q^2$, and $\delta\omega_r^-/\omega_r \approx -C_q^-/(2C_r)$. For the quantum dots we use the parameters of [60, 61], with a tunneling amplitude of $t_c = 23\,\mu$eV. We take an exchange energy J for each qubit which oscillates from $\sim$1 to $\sim$2.5 μ eV, corresponding to electrode voltages from -0.7 to -0.4 mV, dE^-/dV_e from 0.002 to 0.01e, and $C_q^- = 2C_q^+ \sim$1 to 10 aF.

D.3. Trapped molecular ions

Figure 2(d): the trapped polar molecular ions of [3] have a vector dipole moment, associated here primarily with the $J = 1$ excited molecular rotational manifold with sublevels $m_J = -1, 0, 1$ which are degenerate at zero electric field. An electric field shifts the $J = 1, m_J = \pm 1$ levels down, so that a qubit can be realized with the $J = 0, m_J = 0$ and $J = 1, m_J = 0$ states. We therefore cannot simply oscillate the electric field through zero, since the $m_J = 0$ state will undergo Majorana-like transitions to the $m_J = \pm 1$ states near zero field (equivalently, the induced dipole's orientation will not 'follow' the applied field). Instead, we can use a *rotating* electric field E_m with angular frequency ω_m, whose plane of rotation contains the resonator mode field axis as shown in figure D.1(a). In this case, as long as the rotation is not too fast, the molecular dipole will follow it, resulting in an oscillating projection of the dipole along the resonator mode field. The effect of the rotation can be expressed via Larmor's theorem as an effective magnetic field along the rotation axis: $B_{rot} = \hbar\omega_m/\gamma_{J=1}$ where $\gamma_{J=1}$ is the gyromagnetic ratio of the $J = 1$ manifold. As long as the rotation is turned on and off slowly, and we restrict ourselves to $\hbar\omega_m \lesssim E_{m_J=0} - E_{m_J=\pm 1}$, the states will transform adiabatically.

With this in mind, we take $E_m = 2.5\,\mathrm{kV\,cm^{-1}}$, corresponding to a differential stark shift between the $J = 0, m_J = 0$ and $J = 1, m_J = 0$ rotational states from their zero-field splitting of 9 to $\sim$13 GHz, and a splitting between $J = 1, m_J = 0$ and $J = 1, m_J = \pm 1$ of $\sim$ 3 GHz; we take a distance $l = 1\,\mu$m between the qubits and modulation electrodes, so that $V_b \sim E_m l$.

Finally, although the rotation at constant field magnitude E_m does not couple the $J = 0$, $m_J = 0$ to the $J = 1$ manifold, there is a residual direct Jaynes–Cummings type coupling between the resonator and the $J = 0 \leftrightarrow J = 1$ transition, given by: $\hbar g \approx (d_{01}/l)\sqrt{\hbar Y_r}/C_r = 0.4\,\mathrm{MHz}$ ($d_{01} \approx 2.5 \times 10^{-29}\,\mathrm{Cm}$ is the transition dipole between $J = 0$ and 1); this produces a negligible effect at the large qubit–resonator detunings $\gtrsim$10 GHz considered here.

D.4. Donor electron spins in Si

Figure 2(e): Similar to the case of quantum dots and molecular ions which are biased with a voltage or electric field rather than a charge, an electron spin is biased with a magnetic field rather than a flux. In this case, we have: $\eta_0^- \equiv (\mathrm{d}E^-/\mathrm{d}I_q)/(2\sqrt{\hbar Z_r})$, $L_q^- \equiv \mathrm{d}^2E^-/\mathrm{d}I_q^2$ and $\delta\omega_r^-/\omega_r \approx -L_q^-/(2L_r)$. We take a circular loop of diameter $d = 50\,\mathrm{nm}$ connected to the resonator, with the spin at its center, so that the field at the spin is given by: $B_m = \mu_0 I_q/d$. As in the case of molecular ions, a rotating field (turned on and off slowly) must be used to avoid Majorana transitions between spin orientations (figure D.1(b)), whose rotation frequency in this case should be less than the Larmor frequency $\omega_L = \gamma_e B_m/\hbar$. For our modulation at 1 GHz, we then select a field amplitude of $B_m = 1000\,\mathrm{G}$, corresponding to $\omega_L/2\pi = 2.8\,\mathrm{GHz}$. At this field, the hyperfine splitting of $\approx$117 MHz [97] produces a negligible $L_q^- \approx 10^{-22}\mathrm{H}$. Our chosen parameters $Q = 10^7$, $d = 50\,\mathrm{nm}$ and $B_m = 1000\,\mathrm{G}$, while arguably not completely implausible, are admittedly extreme. The very weak interaction with a single spin dictates that such parameters are required for favorable gate parameters. One way to relax these requirements to some extent would be to implement a multiturn coil (it would need to be at the $\sim$100 nm scale) to increase the coupling, or to use an ensemble of spins as a qubit.

D.5. Nitrogen vacancy centers in diamond

Figure 2(f): this case is similar to the electron spin just discussed, except that the system is a spin triplet with $S = 1$, and the $m_S = 0$ state is shifted relative to the $m_S = \pm 1$ states due to crystal-field and magnetic-dipole interactions by 2.88 GHz [98]. The axis of this internal field is fixed by the crystal, so that the alignment of the states cannot follow the external modulation field direction for weak fields. However, if we align the resonator mode field along the NV center's crystal axis, and use a modulation field rotation plane that also contains this axis (figure D.1(c)), we can still realize the desired effect (we take as above $B_m = 1000\,\mathrm{G}$). When the modulation field B_m is along the crystal axis, the resonator field produces a linear Zeeman shift of the $m_S = \pm 1$ states; when the modulation field is perpendicular to the axis, it mixes all three sublevels, producing a large enough avoided crossing that the $m_S = \pm 1$ states can be nearly adiabatically transformed into each other by the modulation, and we can use them as our two qubit states (note that in experiments, the $S = 0, m_S = 0$ state is typically used as $|g\rangle$). As above, this can be fully accounted for using an effective field associated with the rotation. As long as the modulation frequency is not too large, and the modulation is as above turned on and off slowly, nonadiabatic transitions can be neglected at the error levels of interest here.

References

[1] Buluta I, Ashhab S and Nori F 2011 Natural and artificial atoms for quantum computation *Rep. Prog. Phys.* **74** 104401

[2] Xiang Z-L, Ashhab S, You J Q and Nori F 2013 Hybrid quantum circuits: superconducting circuits interacting with other quantum systems *Rev. Mod. Phys.* **85** 623–53

[3] Schuster D I, Bishop L S, Chuang I L, DeMille D and Schoelkopf R J 2011 Cavity QED in a molecular ion trap *Phys. Rev.* A **83** 012311

[4] Andre A, DeMille D, Doyle J M, Lukin M D, Maxwell S E, Rabl P, Schoelkopf R J and Zoller P 2006 A coherent all-electrical interface between polar molecules and mesoscopic superconducting resonators *Nature Phys.* **2** 636–42

[5] Hogan S D, Agner J A, Merkt F, Thiele T, Filipp S and Wallraff A 2012 Driving Rydberg–Rydberg transitions from a coplanar microwave waveguide *Phys. Rev. Lett.* **108** 063004

[6] Guerlin C, Brion E, Esslinger T and Mølmer K 2010 Cavity quantum electrodynamics with a Rydberg-blocked atomic ensemble *Phys. Rev.* A **82** 053832

[7] Petrosyan D, Bensky G, Kurizki G, Mazets I, Majer J and Schmiedmayer J 2009 Reversible state transfer between superconducting qubits and atomic ensembles *Phys. Rev.* A **79** 040304

[8] Sørensen A S, van der Wal C H, Childress L I and Lukin M D 2004 Capacitive coupling of atomic systems to mesoscopic conductors *Phys. Rev. Lett.* **92** 063601

[9] Raimond J M, Brune M and Haroche S 2001 Manipulating quantum entanglement with atoms and photons in a cavity *Rev. Mod. Phys.* **73** 565–82

[10] Blais A, Huang R-S, Wallraff A, Girvin S M and Schoelkopf R J 2004 Cavity quantum electrodynamics for superconducting electrical circuits: an architecture for quantum computation *Phys. Rev.* A **69** 062320

[11] Schuster D I, Wallraff A, Blais A, Frunzio L, Huang R-S, Majer J, Girvin S M and Schoelkopf R J 2005 ac Stark shift and dephasing of a superconducting qubit strongly coupled to a cavity field *Phys. Rev. Lett.* **94** 123602

[12] Wallraff A, Schuster D I, Blais A, Frunzio L, Huang R-S, Majer J, Kumar S, Girvin S M and Schoelkopf R J 2004 Strong coupling of a single photon to a superconducting qubit using circuit quantum electrodynamics *Nature* **431** 162–7

[13] Nori F and You J Q 2011 Atomic physics and quantum optics using superconducting circuits *Nature* **474** 589–97

[14] Schuster D I *et al* 2010 High-cooperativity coupling of electron-spin ensembles to superconducting cavities *Phys. Rev. Lett.* **105** 140501

[15] Bushev P, Feofanov A K, Rotzinger H, Protopopov I, Cole J H, Wilson C M, Fischer G, Lukashenko A and Ustinov A V 2011 Ultralow-power spectroscopy of a rare-earth spin ensemble using a superconducting resonator *Phys. Rev.* B **84** 060501

[16] Miller R, Northup T E, Birnbaum K M, Boca A, Boozer A D and Kimble H J 2005 Trapped atoms in cavity QED: coupling quantized light and matter *J. Phys. B: At. Mol. Opt. Phys.* **38** S551

[17] Walls D F and Milburn G J 1994 *Quantum Optics* (Berlin: Springer)

[18] Sillanpää M A, Park J I and Simmonds R W 2007 Coherent quantum state storage and transfer between two phase qubits via a resonant cavity *Nature* **449** 438–42

[19] Srinivasan S J, Hoffman A J, Gambetta J M and Houck A A 2011 Tunable coupling in circuit quantum electrodynamics using a superconducting charge qubit with a *v*-shaped energy level diagram *Phys. Rev. Lett.* **106** 083601

[20] de Groot P C, Lisenfeld J, Schouten R N, Ashhab S, Lupascu A, Harmans C J P M and Mooij J E 2010 Selective darkening of degenerate transitions demonstrated with two superconducting quantum bits *Nature Phys.* **6** 763–6

[21] Chow J M *et al* 2011 Simple all-microwave entangling gate for fixed-frequency superconducting qubits *Phys. Rev. Lett.* **107** 080502

[22] Leek P J, Filipp S, Maurer P, Baur M, Bianchetti R, Fink J M, Göppl M, Steffen L and Wallraff A 2009 Using sideband transitions for two-qubit operations in superconducting circuits *Phys. Rev.* B **79** 180511
[23] Poletto S *et al* 2012 Entanglement of two superconducting qubits in a waveguide cavity via monochromatic two-photon excitation *Phys. Rev. Lett.* **109** 240505
[24] Lucero E *et al* 2012 Computing prime factors with a Josephson phase qubit quantum processor *Nature Phys.* **8** 719–23
[25] Reed M D, DiCarlo L, Nigg S E, Sun L, Frunzio L, Girvin S M and Schoelkopf R J 2012 Realization of three-qubit quantum error correction with superconducting circuits *Nature* **482** 382–5
[26] Helmer F, Mariantoni M, Fowler A G, von Delft J, Solano E and Marquardt F 2009 Cavity grid for scalable quantum computation with superconducting circuits *Europhys. Lett.* **85** 50007
[27] Galiautdinov A, Korotkov A N and Martinis J M 2012 Resonator zero-qubit architecture for superconducting qubits *Phys. Rev.* A **85** 042321
[28] DiVincenzo D 2009 Fault-tolerant architectures for superconducting qubits *Phys. Scr.* **2009** 014020
[29] Kerman A J 2010 Metastable superconducting qubit *Phys. Rev. Lett.* **104** 027002
[30] Sears A P, Petrenko A, Catelani G, Sun L, Paik H, Kirchmair G, Frunzio L, Glazman L I, Girvin S M and Schoelkopf R J 2012 Photon shot noise dephasing in the strong-dispersive limit of circuit QED *Phys. Rev.* B **86** 180504
[31] Filipp S, Göppl M, Fink J M, Baur M, Bianchetti R, Steffen L and Wallraff A 2011 Multimode mediated qubit–qubit coupling and dark-state symmetries in circuit quantum electrodynamics *Phys. Rev.* A **83** 063827
[32] Rigetti C *et al* 2012 Superconducting qubit in a waveguide cavity with a coherence time approaching 0.1 ms *Phys. Rev.* B **86** 100506
[33] You J Q, Tsai J S and Nori F 2002 Scalable quantum computing with Josephson charge qubits *Phys. Rev. Lett.* **89** 197902
[34] Averin D V and Bruder C 2003 Variable electrostatic transformer: controllable coupling of two charge qubits *Phys. Rev. Lett.* **91** 057003
[35] Hutter C, Makhlin Y, Shnirman A and Schön G 2007 Stability of longitudinal coupling for Josephson charge qubits *Phys. Rev.* B **76** 024512
[36] Liu Y-X, Wei L F, Johansson J R, Tsai J S and Nori F 2007 Superconducting qubits can be coupled and addressed as trapped ions *Phys. Rev.* B **76** 144518
[37] Kerman A J and Oliver W D 2008 High-fidelity quantum operations on superconducting qubits in the presence of noise *Phys. Rev. Lett.* **101** 070501
[38] Wang Y-D, Kemp A and Semba K 2009 Coupling superconducting flux qubits at optimal point via dynamic decoupling with the quantum bus *Phys. Rev.* B **79** 024502
[39] Vacanti G, Fazio R, Kim M S, Palma G M, Paternostro M and Vedral V 2012 Geometric-phase backaction in a mesoscopic qubit–oscillator system *Phys. Rev.* A **85** 022129
[40] Leibfried D *et al* 2003 Experimental demonstration of a robust, high-fidelity geometric two ion-qubit phase gate *Nature* **422** 412–5
[41] Haljan P C, Brickman K-A, Deslauriers L, Lee P J and Monroe C 2005 Spin-dependent forces on trapped ions for phase-stable quantum gates and entangled states of spin and motion *Phys. Rev. Lett.* **94** 153602
[42] Mølmer K and Sørensen A 1999 Multiparticle entanglement of hot trapped ions *Phys. Rev. Lett.* **82** 1835–8
[43] Sørensen A and Mølmer K 2000 Entanglement and quantum computation with ions in thermal motion *Phys. Rev.* A **62** 022311
[44] Milburn G J, Schneider S and James D F V 2000 Ion trap quantum computing with warm ions *Fortschr. Phys.* **48** 801–10
[45] Leghtas Z, Kirchmair G, Vlastakis B, Devoret M H, Schoelkopf R J and Mirrahimi M 2013 Deterministic protocol for mapping a qubit to coherent state superpositions in a cavity *Phys. Rev.* A **87** 042315
[46] Pechal M, Berger S, Abdumalikov A A, Fink J M, Mlynek J A, Steffen L, Wallraff A and Filipp S 2012 Geometric phase and nonadiabatic effects in an electronic harmonic oscillator *Phys. Rev. Lett.* **108** 170401

[47] Likharev K K 1987 Single-electron transistors: electrostatic analogs of the dc SQUIDS *IEEE Trans. Magn.* **23** 1142
[48] Kadin A M 1990 Duality and fluxonics in superconducting devices *J. Appl. Phys.* **68** 5741–9
[49] Mooij J E and V Nazarov Yu 2006 Superconducting nanowires as quantum phase-slip junctions *Nature Phys.* **2** 169–72
[50] Kerman A J 2013 Flux-charge duality and topological quantum phase fluctuations in quasi-one-dimensional superconductors *New J. Phys.* **15** 105017
[51] Likharev K K and Zorin A B 1985 Theory of the Bloch-wave oscillations in small Josephson junctions *J. Low Temp. Phys.* **59** 347–82
[52] Guichard W and Hekking F W J 2010 Phase-charge duality in Josephson junction circuits: role of inertia and effect of microwave irradiation *Phys. Rev.* B **81** 064508
[53] Devoret M H 1997 Quantum fluctuations in electrical circuits *Quantum Fluctuations* ed S Reynaud, E Giacobino and J Zinn-Justin (Amsterdam: Elsevier) pp 351–86
[54] Lupaşcu A, Verwijs C J M, Schouten R N, Harmans C J P M and Mooij J E 2004 Nondestructive readout for a superconducting flux qubit *Phys. Rev. Lett.* **93** 177006
[55] Duty T, Johansson G, Bladh K, Gunnarsson D, Wilson C and Delsing P 2005 Observation of quantum capacitance in the cooper-pair transistor *Phys. Rev. Lett.* **95** 206807
[56] Sillanpää M A, Lehtinen T, Paila A, Makhlin Yu, Roschier L and Hakonen P J 2005 Direct observation of Josephson capacitance *Phys. Rev. Lett.* **95** 206806
[57] Paauw F G, Fedorov A, Harmans C J P M and Mooij J E 2009 Tuning the gap of a superconducting flux qubit *Phys. Rev. Lett.* **102** 090501
[58] Gustavsson S, Bylander J, Yan F, Oliver W D, Yoshihara F and Nakamura Y 2011 Noise correlations in a flux qubit with tunable tunnel coupling *Phys. Rev.* B **84** 014525
[59] Orlando T P, Mooij J E, Tian L, van der Wal C H, Levitov L S, Lloyd S and Mazo J J 1999 Superconducting persistent-current qubit *Phys. Rev.* B **60** 15398–413
[60] Petta J R, Johnson A C, Taylor J M, Laird E A, Yacoby A, Lukin M D, Marcus C M, Hanson M P and Gossard A C 2005 Coherent manipulation of coupled electron spins in semiconductor quantum dots *Science* **309** 2180–4
[61] Laird E A, Petta J R, Johnson A C, Marcus C M, Yacoby A, Hanson M P and Gossard A C 2006 Effect of exchange interaction on spin dephasing in a double quantum dot *Phys. Rev. Lett.* **97** 056801
[62] Maune B M *et al* 2012 Coherent singlet-triplet oscillations in a silicon-based double quantum dot *Nature* **481** 169–72
[63] Shulman M D, Dial O E, Harvey S P, Bluhm H, Umansky V and Yacoby A 2012 Demonstration of entanglement of electrostatically coupled singlet-triplet qubits *Science* **336** 202–5
[64] Steger M, Saeedi K, Thewalt M L W, Morton J J L, Riemann H, Abrosimov N V, Becker P and Pohl H-J 2012 Quantum information storage for over 180 s using donor spins in a ^{28}Si 'semiconductor vacuum' *Science* **336** 1280–3
[65] Balasubramanian G *et al* 2009 Ultralong spin coherence time in isotopically engineered diamond *Nature Mater.* **8** 383–7
[66] Bishop L S, Ginossar E and Girvin S M 2010 Response of the strongly driven Jaynes–Cummings oscillator *Phys. Rev. Lett.* **105** 100505
[67] Šašura M and Steane A M 2003 Fast quantum logic by selective displacement of hot trapped ions *Phys. Rev.* A **67** 062318
[68] Palacios-Laloy A, Mallet F, Nguyen F, Ong F, Bertet P, Vion D and Esteve D 2009 Spectral measurement of the thermal excitation of a superconducting qubit *Phys. Scr.* **T137** 014015
[69] Corcoles A D, Chow J M, Gambetta J M, Rigetti C, Rozen J R, Keefe G A, Rothwell M B, Ketchen M B and Steffen M 2011 Protecting superconducting qubits from radiation *Appl. Phys. Lett.* **99** 181906
[70] Ithier G *et al* 2005 Decoherence in a superconducting quantum bit circuit *Phys. Rev.* B **72** 134519

[71] Biercuk M J, Uys H, Van Devender A P, Shiga N, Itano W M and Bollinger J J 2009 Optimized dynamical decoupling in a model quantum memory *Nature* **458** 996–1000
[72] Bylander J, Gustavsson S, Yan F, Yoshihara F, Harrabi K, Fitch G, Cory D G, Nakamura Y, Tsai J-S and Oliver W D 2011 Noise spectroscopy through dynamical decoupling with a superconducting flux qubit *Nature Phys.* **7** 565–70
[73] Houck A A *et al* 2008 Controlling the spontaneous emission of a superconducting transmon qubit *Phys. Rev. Lett.* **101** 080502
[74] Kerman A J, Dauler E A, Keicher W E, Yang J K W, Berggren K K, Gol'tsman G and Voronov B 2006 Kinetic-inductance-limited reset time of superconducting nanowire photon counters *Appl. Phys. Lett.* **88** 111116
[75] Barends R, Vercruyssen N, Endo A, de Visser P J, Zijlstra T, Klapwijk T M, Diener P, Yates S J C and Baselmans J J A 2010 Minimal resonator loss for circuit quantum electrodynamics *Appl. Phys. Lett.* **97** 023508
[76] Kamlapure A, Mondal M, Chand M, Mishra A, Jesudasan J, Bagwe V, Benfatto L, Tripathi V and Raychaudhuri P 2010 Measurement of magnetic penetration depth and superconducting energy gap in very thin epitaxial NbN films *Appl. Phys. Lett.* **96** 072509
[77] Baek B, Lita A E, Verma V and Nam S W 2011 Superconducting a-W_xSi_{1-x} nanowire single-photon detector with saturated internal quantum efficiency from visible to 1850 nm *Appl. Phys. Lett.* **98** 251105
[78] Sandberg M, Vissers M R, Kline J S, Weides M, Gao J, Wisbey D S and Pappas D P 2012 Etch induced microwave losses in titanium nitride superconducting resonators *Appl. Phys. Lett.* **100** 262605
[79] Megrant A *et al* 2012 Planar superconducting resonators with internal quality factors above one million *Appl. Phys. Lett.* **100** 113510
[80] Barreiro J T, Muller M, Schindler P, Nigg D, Monz T, Chwalla M, Hennrich M, Roos C F, Zoller P and Blatt R 2011 An open-system quantum simulator with trapped ions *Nature* **470** 486–91
[81] Neeley M *et al* 2010 Generation of three-qubit entangled states using superconducting phase qubits *Nature* **467** 570–3
[82] DiCarlo L, Reed M D, Sun L, Johnson B R, Chow J M, Gambetta J M, Frunzio L, Girvin S M, Devoret M H and Schoelkopf R J 2010 Preparation and measurement of three-qubit entanglement in a superconducting circuit *Nature* **467** 574–8
[83] Tsomokos D I, Ashhab S and Nori F 2008 Fully connected network of superconducting qubits in a cavity *New J. Phys.* **10** 113020
[84] Galiautdinov A, Coffey M W and Deiotte R 2009 Greenberger–Horne–Zeilinger state protocols for fully connected qubit networks *Phys. Rev.* A **80** 062302
[85] Kuznetsova E, Bragdon T, Côté R and Yelin S F 2012 Cluster-state generation using van der Waals and dipole–dipole interactions in optical lattices *Phys. Rev.* A **85** 012328
[86] Casanova J, Mezzacapo A, Lamata L and Solano E 2012 Quantum simulation of interacting fermion lattice models in trapped ions *Phys. Rev. Lett.* **108** 190502
[87] Raussendorf R and Harrington J 2007 Fault-tolerant quantum computation with high threshold in two dimensions *Phys. Rev. Lett.* **98** 190504
[88] Kovalev A A and Pryadko L P 2013 Fault tolerance of quantum low-density parity check codes with sublinear distance scaling *Phys. Rev.* A **87** 020304
[89] Slichter D H, Vijay R, Weber S J, Boutin S, Boissonneault M, Gambetta J M, Blais A and Siddiqi I 2012 Measurement-induced qubit state mixing in circuit QED from up-converted dephasing noise *Phys. Rev. Lett.* **109** 153601
[90] Wieman C E, Pritchard D E and Wineland D J 1999 Atom cooling, trapping and quantum manipulation *Rev. Mod. Phys.* **71** S253–62
[91] Miller J D, Cline R A and Heinzen D J 1993 Far-off-resonance optical trapping of atoms *Phys. Rev.* A **47** R4567–70
[92] Gunnarsson D, Tuorila J, Paila A, Sarkar J, Thuneberg E, Makhlin Y and Hakonen P 2008 Vibronic spectroscopy of an artificial molecule *Phys. Rev. Lett.* **101** 256806

[93] Hite D A *et al* 2012 100-fold reduction of electric-field noise in an ion trap cleaned with *in situ* argon-ion-beam bombardment *Phys. Rev. Lett.* **109** 103001

[94] Gilchrist A, Langford N K and Nielsen M A 2005 Distance measures to compare real and ideal quantum processes *Phys. Rev.* A **71** 062310

[95] Anglin J R and Zurek W H 1996 Decoherence of quantum fields: pointer states and predictability *Phys. Rev.* D **53** 7327–35

[96] Paraoanu Gh-S and Scutaru H 1998 Bures distance between two displaced thermal states *Phys. Rev.* A **58** 869–71

[97] Thewalt M L W *et al* 2007 Direct observation of the donor nuclear spin in a near-gap bound exciton transition: ^{31}P in highly enriched ^{28}Si *J. Appl. Phys.* **101** 081724

[98] Wrachtrup J, Kilin S Ya and Nizovtsev A P 2001 Quantum computation using the ^{13}C nuclear spins near the single NV defect center in diamond *Opt. Spectrosc.* **91** 429–37